ISSN 1995-0780, Nanotechnologies in Russia, 2009, Vol. 4, Nos. 7–8, pp. 425–447. © Pleiades Publishing, Ltd., 2009.
Original Russian Text © V.I. Balykin, P.N. Melent'ev, 2009, published in Rossiiskie nanotekhnologii, 2009, Vol. 4, Nos. 7–8.

REVIEWS

Nanolithography with Atom Optics

V. I. Balykin and P. N. Melent'ev

Institute of Spectroscopy, Russian Academy of Sciences, ul. Fizicheskaya 5, Troitsk, Moscow oblast, 142190 Russia
e-mail: balykin@isan.troitsk.ru

R

Abstract—Basic results obtained in atom optics, which is a rapidly developing new field of particle optics, and atom nanolithography, which is one of its practical applications, are presented. Basic methods for creating elements of atom optics are considered, the main achievements of atom optics-based atom nanolithography are presented, and prospects for atom nanolithography development are discussed.

DOI: 10.1134/S1995078009070040

INTRODUCTION

Nanolithography is an interdisciplinary field of scientific and applied research with the objective of creating material structures with dimensions from a single atom to about 100 nm. The creation of structures with such dimensions is of practical value and fundamental interest, because structures with dimensions around 10 nm form the bridge between classical and quantum worlds [1]. The stimulating factor in the development of nanolithography is the "race" for an increased number of transistors in the chip described by Moore's law (Moore, 1965) (Fig. 1). According to Moore's law, the number of transistors in new microchips increases by a factor of 2 every 18–24 months, which results in an increase in their functionality and performance and a decrease in the cost of each transistor.

Methods of optical lithography using far vacuum-ultraviolet radiation [2, 3] (methods of lithography using electron and ion beams and X-rays [4–6]) are being successfully developed. These methods provide for the creation of nanostructures with a precision of several nanometers. At the same time, there is a broad

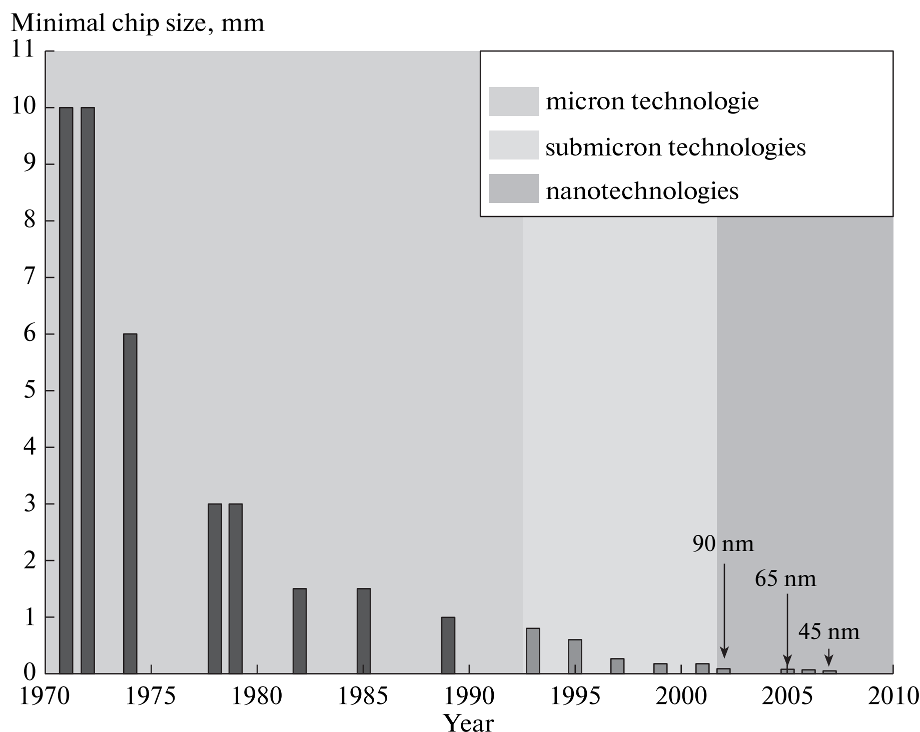

Fig. 1. According to Moore's law, the number of transistors in new microchip models increases by a factor of 2 each 18–24 months. The figure shows the minimal size of the Intel chip element as a function of the production year.

Optics type	Wavelength range 1 mm 1 nm 0.1 E 10^{-14} m	Applied interaction types
Photon	visible light UV EUV X-rays	light with matter
Atom	neutral atoms	atom with laser, electric, and magnetic fields
Neutron	neutrons	neutron with nucleus
Charged particles	electrons ions	moving electrons and ions with magnetic and electric fields

Fig. 2. Table illustrates (1) different types of photon and particle optics (electron, ion, neutron, and atom optics), (2) wavelength range corresponding to a particular optics type, and (3) interaction used in the construction of a particular optics type.

search for alternative methods (such as the scanning nanoprobe method [7], “imprinting” method [8], and the “self-assembly” of nanostructures [9]). It is in this context of a search for alternative future methods of nanolithography that the approaches based on atom-optics methods discussed below should be considered.

Atom optics formed into a separate physical discipline in the mid-1980s as a result of investigating the influence of the forces of laser light pressure on the forward movement of atoms. Atom optics, similar to electron, ion, and neutron optics, is related to particle optics (Fig. 2) and considers the problems of the formation and control of ensembles and beams of neutral atoms and their application. The development of atom optics [10–13] is closely connected with the development of methods of laser cooling and localization of neutral atoms [14–18]. The laser cooling of atoms and their spatial localization form atomic ensembles and beams with given parameters. Laser cooling provides a decrease in the atomic temperature to about several μK. At such temperatures the De Broglie wavelength becomes comparable to the light wavelength and the wave properties of atoms begin to manifest. The localization of neutral atoms opens up the possibilities of operating with both single atoms localized with a nanometer precision [19, 20] and macroscopic ensembles of cold atoms with high phase density [21]. Based on different configurations of laser light fields and mechanical micro- and nanostructures (zone plates, multislit diaphragms, etc.), many atom optics elements have been created: lenses, mirrors; coherent atomic beam splitters; atomic interferometers; waveguides; and finally, an atom laser, which is an analogue to the optical laser. The capabilities of atom optics are much broader than other types of particle (electron and neutron) optics due to the internal structure of the atom. At a temperature close to absolute zero, when the De Broglie wavelength becomes comparable to the interatomic distance, the behavior of the atomic ensemble begins to noticeably depend on the internal quantum characteristic of the atom (its spin). The most striking difference between the behavior of fermions and bosons is observed at very low temperatures. For bose particles, a condensation phenomenon is observed at ultralow temperatures which was called Bose–Einstein condensation (BEC). Atoms in the BEC state form a new type of “coherent matter” [21]. The magnetic trap keeping BEC atoms is analogous to an optical resonator for photons in an optical laser. Atoms can be “released” from the magnetic trap in a certain direction (similarly to photons through a semitransparent mirror of the optical resonator of a laser), and they form a coherent directed beam similar to a laser beam. Such a device is called an atom laser. The great interest in atom lasers is due to the potential capability of using coherent atomic beams in high-precision measuring devices and high technologies upon the creation of atomic and molecular micro- and nanostructures [19, 20].

The objective of this survey is to make an introduction into the quickly developing new type of particle optics (atom optics) and one of its practical applications (atom nanolithography). Basic methods for creating atom optics elements based on matter structures, static magnetic and electric fields, and laser radiation are described briefly in Section 2. The main achievements of atom optics-based atom nanolithography are presented in Section 3. In the Conclusion, the prospects of developing atom nanolithography are discussed.

ATOM OPTICS: METHODS FOR CONSTRUCTING THE BASIC ELEMENTS

Although atom and light optics have similar mathematical grounds, their “technical tools” are different. Light optics is based on the technology of polishing the surface of a required shape from different reflecting and transparent materials. In atom optics the main “technical tools” are electromagnetic fields. The application of various configurations of static electric and magnetic fields, laser fields, and matter structures

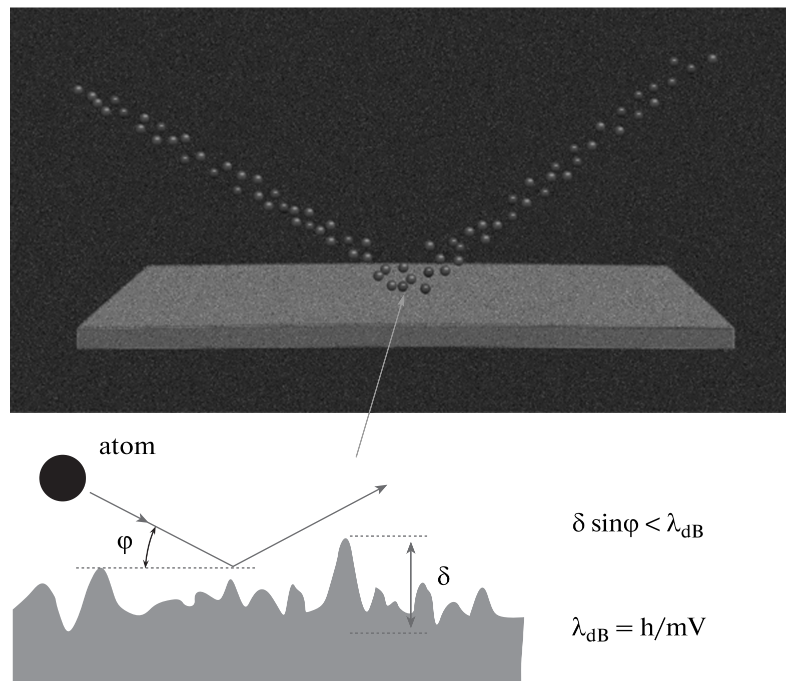

Fig. 3. The surface of a solid as an atom optics element (atom mirror).

(micro- and nanostructures) provided for the construction of basic elements of atom optics that are similar to the elements of common optics.

ATOM OPTICS ELEMENTS BASED ON MATTER STRUCTURES

The simplest element of atom optics is the surface of a solid. In classical monograph [22], the specular reflection and diffraction of a molecular beam from the surface of a solid were considered. The following two conditions should be satisfied for specular reflection:

(a) the projection of the average height of the surface irregularity onto the direction of the molecular beam should be smaller than the De Broglie wavelength of the molecule (Fig. 3). If δ is the average height of the surface irregularities and φ is the sliding angle of the incident beam, this requirement can be written as

$$\delta \sin\varphi < \lambda_{bB}; \qquad (1)$$

(b) the average time that the molecule spends on the surface should be short. In this case the quantum state of the reflected molecule is the same as that of the incident molecule. Irregularities of well mechanically polished surfaces are usually around 10^{-5} cm, while the De Broglie wavelength of the hydrogen molecule at 300 K is around 10^{-8} cm. Therefore, according to relation (1), the specular reflection angle should satisfy the condition $\varphi < 10^{-3}$ rad.

The 5% reflection of the beam of hydrogen molecules from polished bronze for the sliding incidence angle $\varphi = 10^{-3}$ rad was observed more than 80 years ago [23]. The crystal cleavage surfaces are much smoother. Thermal oscillations of the crystalline lattice are limited by the surface “smoothness” on a level of 10^{-8} cm. In this case the atomic beam is reflected specularly for 20–30° angles of incidence. This was testified in experiments [24] with He atoms and LiF crystal. The temperature dependence of the specular reflection angle has a sharp transition from specular to diffuse reflection of atoms, which testifies to the influence of thermal oscillations on the “smoothness” of the crystal surface. Experiments on the reflection of atoms from the surface of the condensed medium still attract the attention of researchers. The following experiments should be pointed out: experiments on the reflection of ^{4}He atoms from the surface of liquid ^{4}He [25] and thermal Cs atoms incident on polished glass surface [26].

The first experiment on observing the diffraction of atoms on the crystal cleavage surface acting as a 2D plane lattice was performed by Stern [27]; the results of detailed study of this phenomenon were presented in [28]. The diffraction of atoms on an artificial periodic structure (cuts in a membrane) with a much larger lattice period was observed in [29].

The effect of the quantum reflection of beams of ^{4}He and ^{3}He atoms from the surface of liquid helium in a vacuum was successfully used for focusing atoms of concave surface [30], and in [31] the experiment on focusing He atoms by a zone plate (Fig. 4) was successfully performed. In [32] the zone plate-based microscope was first presented; in this microscope the

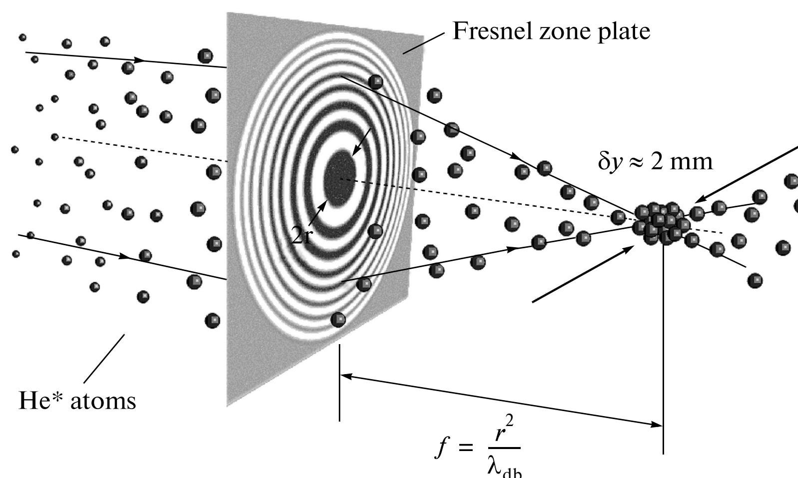

Fig. 4. Schematic diagram of atomic beam focusing by zone plate [31].

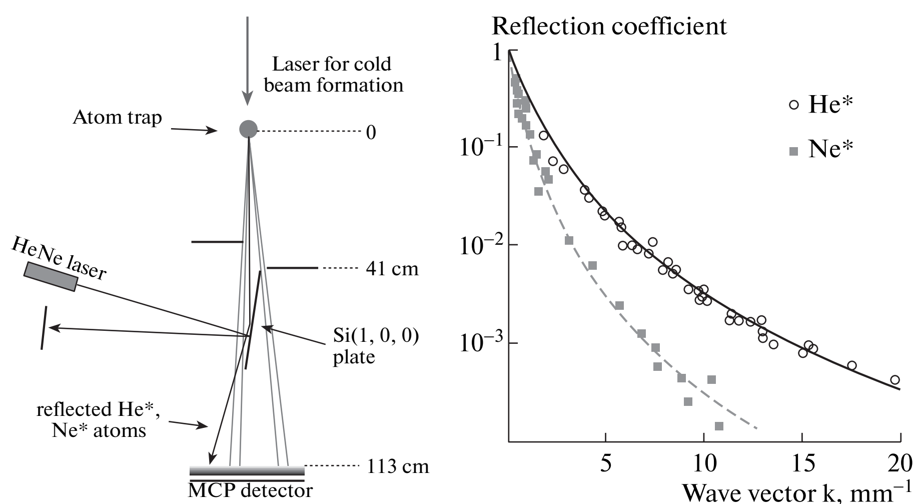

Fig. 5. Schematic diagram on quantum reflection of metastable Ne atoms from a silicon surface [33]. The beam of slow Ne or He atoms is formed by their acceleration by laser light from the atom trap. Reflected atoms are registered using MCP detector. The reflection coefficient as a function of the wave vector of an atom wave is shown on the right.

image of a 2D object was created using metastable He atoms. The obtained resolution was about 1 μm.

The development of the method of laser cooling of atoms provided for the handling of slow-atom beams with a rather large De Broglie wavelength. According to the laws of quantum mechanics, such atoms can experience reflection from a strong potential drop independently of its sign. This takes place if the change of the wave vector of the incident particle exceeds the initial value of the wave vector on the scale of the De Broglie wavelength of the particle. In [33] the specular reflection of Ne atoms from the Si (1, 0, 0) surface was demonstrated for extremely low atomic velocities (v = 1 mm/s) for which Casimir and van der Waals forces considerably influence the character of atom reflection. The reflection coefficient reached 50% (Fig. 5).

Artificial matter microstructures were also used for implementing atomic interferometry in Young [34] and Michelson [35] atomic interferometers.

STATIC ELECTRIC AND MAGNETIC FIELDS IN THE CONSTRUCTION OF ATOM OPTICS ELEMENTS

Some elements of atom and molecule optics based on the interaction between spatially inhomogeneous magnetic or electric fields and the magnetic or electric dipole moments of particles have been known and successfully used in experimental physics for a long time [22].

In the presence of a magnetic or electric field, the position of the atom or molecule shifts and the shift value depends on the initial quantum state of the par-

ticle and the field value (Zeeman and Stark effects). In the adiabatic approximation (fields vary in time and space rather slowly, and particles move sufficiently slowly), the internal particle state follows the changes of the field strength; in other words, particles remain on the same quantum sublevel as the energy W, depending on the field strength.

Magnetic Interaction

For the atom or molecule possessing the constant magnetic moment μ, the effective potential energy W in the external magnetic field with the strength $\mathbf{H}$ is

$$W = -\mu\mathbf{H} = -\mu_{\text{eff}}H, \quad (2)$$

where μ_{eff} is the projection of μ onto the direction of $\mathbf{H}$. The force F acting on the atom or molecule with the potential energy W is

$$\mathbf{F} = -\nabla W = -(\partial W/\partial H)\nabla H = \mu_{\text{eff}}\nabla H. \quad (3)$$

It follows from (3) that the particle in the inhomogeneous magnetic field is influenced by the force directed along the field strength gradient.

Using an inhomogeneous magnetic field for focusing a beam of molecules emitted at different angles from the source was proposed in [36–39].

The focusing properties of magnetic lenses depend on the magnetic sublevels of the atom. This was successfully implemented by Ramsey et al. for creating a hydrogen maser [40]. Hydrogen atoms in the state $F = 1$, $M = 0$ were focused into a small hole in the wall of the accumulating bulb and were accumulated in it, while atoms in the lower state $F = 0$ were defocused.

The potential energy of an atom in a magnetic field and therefore, the force acting on the atom are limited by the Bohr magneton; for magnetic fields available in laboratory conditions, the focal distance of the magnetic lens for thermal atomic beams makes a large value of around 1 m or more. The development of methods of laser cooling and deceleration of atomic beams cardinally changed the situation and provided the implementation of magnetic lenses with a focal distance of around 1 cm, which in turn allowed one to decrease aberrations caused by the non-monochromatic character of atomic beams [41]. In [42] in order to increase the density of the atomic beam used in the experiment on atom nanolithography, the beam of Cs atoms was focused into a spot with a diameter of about 45 μm using a magnetic lens (Fig. 6).

Electric Interaction

Because the energy of an atom or molecule in an electric field depends on the field strength, similarly to (2) and (3) it can be assumed that the atom (molecule) possesses the effective dipole moment,

$$\mu_{\text{eff}} = -(dW/dE). \quad (4)$$

The force acting on the atom (molecule) in the inhomogeneous electric field is determined by an expression similar to (3),

$$\mathbf{F} = \mu_{\text{eff}}\nabla E = \mu_{\text{eff}}(\partial E/\partial Z), \quad (5)$$

where the direction of the field strength gradient is chosen along the Z axis.

Paul et al. [43] created focusing fields for a beam of polar molecules. The electrically focusing the beam of molecules in a certain (excited) quantum state was done by Townes, Basov, and Prokhorov to create NH_3 maser [44, 45]. Focusing a beam of atoms in the ground quantum state, in which the dipole moment is considerably smaller, was studied not long ago. The axially symmetric electrostatic electric field was used [46].

Hexapolar electric fields possess focusing properties and also selectivity with respect to the quantum state of molecules (μ_{eff} depends on the quantum numbers J, K, and M of the molecule). The latter property was successfully used in experiments on molecular dynamics with a beam of molecules in a certain quantum state, including experiments on orienting molecules. In [47] focusing Cs atoms in the ground state into the submillimeter size by a hexagonal electrostatic field was experimentally studied.

LASER FIELDS IN ATOM OPTICS

The behavior of an atom in a laser field is characterized by the electric dipole interaction. When the dipole interacts with the light field $\mathbf{E} = \mathbf{E}(\mathbf{r}, t)$ described by the operator of dipole interaction

$$V = -\mathbf{DE}, \quad (6)$$

the atom acquires the induced dipole moment $\langle\mathbf{D}\rangle$. The induced dipole moment of the atom is determined, as usual, by the quantum mechanical average

$$\langle\mathbf{D}\rangle = \text{Tr}(\rho\mathbf{D}), \quad (7)$$

where ρ is the atomic density matrix. Due to the induced dipole moment of the atom, the spatially inhomogeneous light field $\mathbf{E}(\mathbf{r}, t)$ creates a dipole radiation force acting on the atom.

According to relation (6), the energy of dipole interaction of the atom and the light field is determined as

$$U = \langle V\rangle = -\langle\mathbf{D}\rangle\mathbf{E}. \quad (8)$$

Relation (8) formally coincides with the classical expression for the energy of the interaction between the constant dipole and the electric field $\mathbf{E}$. In this regard, relation (8) can be used to calculate the force acting on the atom in the light field $\mathbf{E}$. The force acting on the particle with the constant dipole moment $\langle\mathbf{D}\rangle$ is determined by the expression

$$\mathbf{F} = \nabla U = \nabla(\langle\mathbf{D}\rangle\mathbf{E}) = \langle D_i\rangle\nabla E_i, \quad (9)$$

where the index $i = x, y, z$ determines the Cartesian coordinates of the vectors.

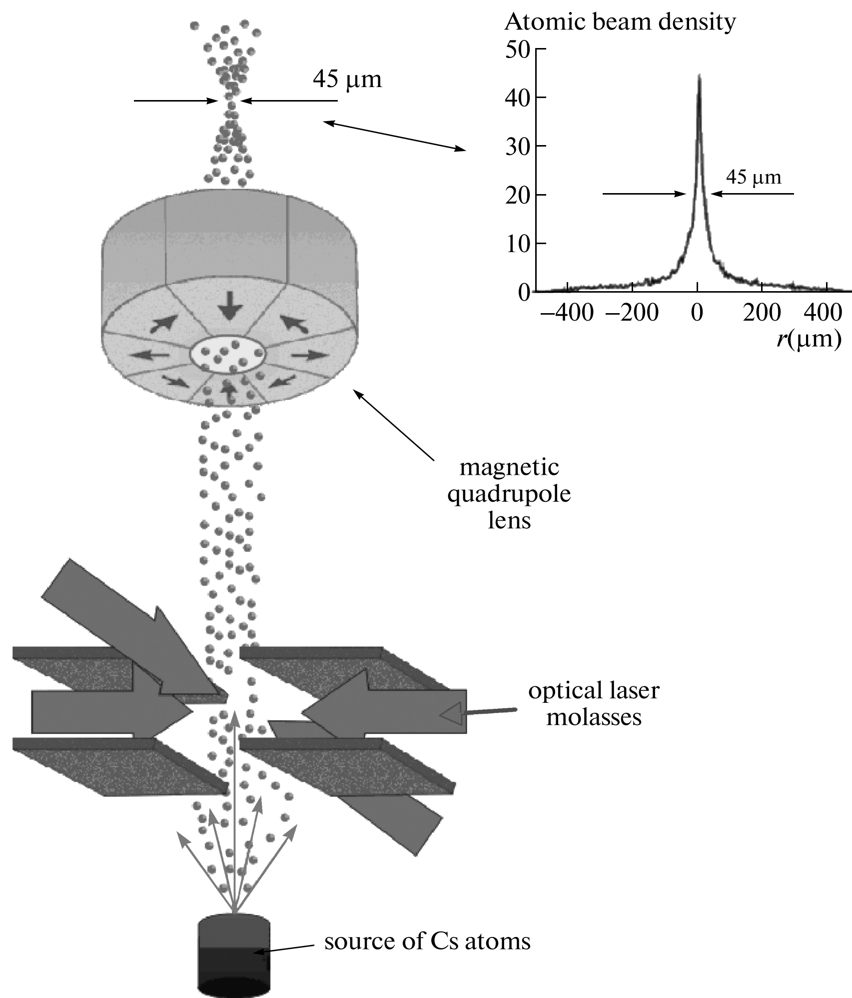

Fig. 6. (Left) Schematic diagram of atom focusing with a magnetic lens and (right) the atomic beam density in the lens focus as a function of transverse coordinate [42].

In atom optics the interaction of a two-level atom with such practically important monochromatic light fields as a laser beam and a standing laser wave is of most interest.

The radiation force acting on the two-level atom in the laser field, according to basic formula (9), is reduced to the sum of two forces: the light pressure force $\mathbf{F}_{lp}$ and the dipole gradient force $\mathbf{F}_{gr}$,

$$\mathbf{F} = \mathbf{F}_{lp} + \mathbf{F}_{gr}, \quad (10)$$

$$\mathbf{F}_{lp} = \hbar\mathbf{k}\gamma\frac{G(\mathbf{r})}{1 + G(\mathbf{r}) + (\delta - \mathbf{kv})^2/\gamma^2}, \quad (11)$$

$$\mathbf{F}_{gr} = -\frac{1}{2}\hbar(\delta - \mathbf{kv})\frac{\nabla G(\mathbf{r})}{1 + G(\mathbf{r}) + (\delta - \mathbf{kv})^2/\gamma^2}, \quad (12)$$

where $G(\mathbf{r})$ is the dimensionless saturation parameter, $G(\mathbf{r}) = \frac{I(\mathbf{r})}{I_S}$, $I(\mathbf{r})$ is the laser radiation intensity at the point $\mathbf{r}$, I_S is the saturation intensity, $\mathbf{k}$ is the wave vector, γ is the half-width of the absorption line of the atomic transition, and δ is the detuning of the laser frequency ω with respect to the atomic transition frequency $\omega_0 : \delta = \omega - \omega_0$. The light pressure force $\mathbf{F}_{lp}$ is due to the interaction of the induced dipole moment of the atom with the light field varying on the wavelength scale ($\lambda = 2\pi/k$). The gradient force $\mathbf{F}_{gr}$ is due to the interaction between the induced dipole moment of the atom and the light field variation on the field amplitude scale.

When there is an interaction between the two-level atom and the laser beam, there is a simple physical interpretation of two parts of the radiation force using the language of elementary processes of photon absorption and emission. The light pressure force occurs as a result of the stimulated absorption of laser photon and the subsequent spontaneous photon emission into one of the modes of the vacuum field. Stimulated photon emission into the same laser mode does not change the laser field momentum or the momentum of the atom. Because the direction of spontaneous photon emission is arbitrary, the momentum trans-

ferred to the atom, averaged over many acts of spontaneous emission, is equal to zero. Thus, the light pressure force occurs as a result of the transfer of the photon momentum to the atom during its stimulated absorption and subsequent spontaneous photon emission. The nature of the light pressure force is dissipative.

If the light field is spatially inhomogeneous, as in the case of the laser beam, the field is the superposition of many plane waves propagating within the laser beam divergence angle. In this relation, in the field of the inhomogeneous beam, the additional elementary process responsible for momentum transfer to the atom is the stimulated absorption by the atom of the photon from one plane light wave and subsequent stimulated emission of the photon into another plane wave of a laser field. Both photons have the same energy and different propagation directions. As a result of this process, the gradient force directed along the laser beam intensity gradient occurs. A gradient force has a potential character due to its origin.

The action of the light pressure and the gradient forces on the atom is quite different. The light pressure force accelerates (decelerates) the atom in the direction of the wave vector **k**. The value and direction of the gradient force depend on the laser beam intensity gradient and the atom velocity along the laser beam. Most of the experiments on the control of atomic motion are based on the use of the gradient and spontaneous force. In atom optics the light pressure force is used for the formation of atomic beams: the improvement of monochromaticity and divergence of atomic beam [48, 49] and the increase in its phase density [50]. Gradient force is used for the construction of atom optics elements: lenses, mirrors, beam splitters, diffraction gratings, and interferometers [10–13].

Atoms and molecules without a static magnetic or electric dipole moment cannot change their mechanical trajectory in a static magnetic or electric field. In this case laser fields are used, because the atom possesses high-frequency polarizability in the quasiresonance high-frequency field and, if the laser field intensity is spatially inhomogeneous, the atom is influenced by the gradient force. For example, the gradient force in the standing laser wave can cause their channeling if there is motion at small angles along the wave front [51, 52], or even trapping cold atoms in a 3D standing light wave [53, 54]. Gradient force was first used by Ashkin et al. for focusing an atomic beam [55] and controlling microparticle motion [56].

ATOM NANOLITHOGRAPHY

In nanolithography neutral atoms possess a certain advantage over photons and particles (ions and electrons). First, neutral atoms have smaller De Broglie wavelengths λ_{dB} than the light wavelength. Second, neutral atoms are not subject to Coulomb repulsion. Third, the methods of laser cooling atoms allow one to control the longitudinal and transverse velocities of atoms, in particular, monochromate and collimate atomic beams, increasing their phase density. The latter means that the Helmholtz–Lagrange law and Liouville's theorem on volume conservation in the phase space, which considerably limit the capabilities of photon and ion optics, are inapplicable for atom optics. All this allows one to effectively control the key parameters of atomic beams by laser light, which is important in creating atomic and molecular nanostructures using methods of atom optics.

ATOM OPTICAL NANOLITHOGRAPHY

Currently, atom optical nanolithography denotes methods for creating atomic nanostructures using laser light. Various laser field configurations are used: running and standing waves of laser fields, as well as spatially localized laser fields. Up to now, the most important results were obtained using standing laser waves. At the same time, it is assumed that spatially localized laser fields possess great perspectives in atom nanolithography. Both types of waves will be considered briefly below.

STANDING WAVE ATOM MICROLENSES

Atom optical lithography is based on using laser light in the formation of nanoatructures on the surface; currently, the greatest achievements have been demonstrated using standing light waves as atom microlenses. Two basic methods were demonstrated: (1) the direct deposition of atoms onto the surface; and (2) lithography using excited (metastable) atoms and chemically active atoms (alkali elements). Surface nanolithography was demonstrated in 1D and 2D cases in the form of regular and more complex structures. Successful demonstrative experiments were performed for many atoms (metastable atoms of noble gases, as well as nonmagnetic and magnetic atoms).

Since the first successful experiments [57, 59], atom optical lithography has became a promising method for creating surface nanostructures. Basic achievements in this field [20, 58–64] are briefly considered below.

The dipole force acting on the atom with the absorption frequency ω_A in the inhomogeneous laser field with the frequency ω_L is determined by the spatial inhomogeneity of the field intensity. In the standing quasiresonance light wave ($\gamma \ll \delta = \omega_L - \omega_A$, $\delta \gg \gamma G^{1/2}$), the resulting force has the form

$$F(x) = -dU(x)/dx = F_{\max}\sin^2 kx, \qquad (13)$$

where $U(x)$ is the potential energy of the atom in the laser field.

A separate atom lens of the standing wave (Fig. 7) has the spatial dimension from $x = -\lambda/4$ to $x = +\lambda/4$. In the neighborhood of the point $x = 0$, the atom experiences harmonic oscillations with the period $T_{\rm osc} =$

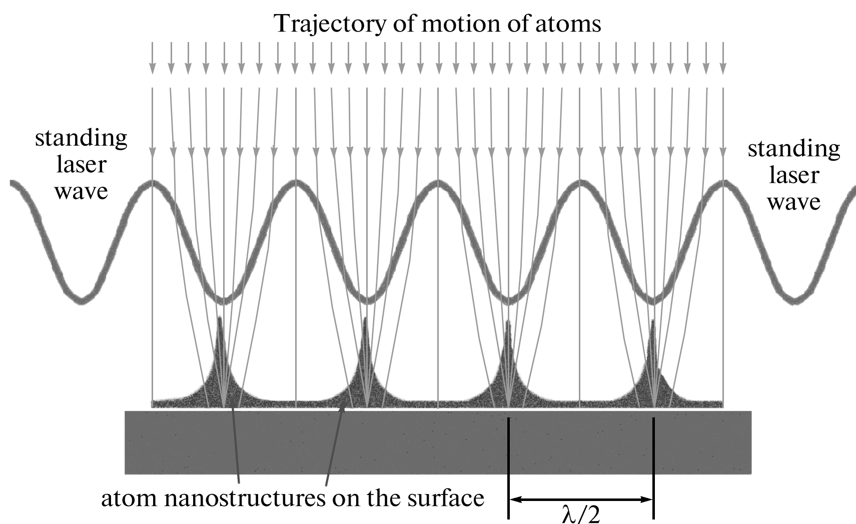

Fig. 7. Atom lens formed by a standing light wave.

$2\pi\sqrt{M/V}$, where $V \equiv \partial^2 U(x)/\partial x^2|_{x=0}$ and M is the mass of the atom. Two limiting types of atom lenses of the standing wave are distinguished. For a "thin lens," the spatial shift of the atom when traversing the lens is small and, after passing through the lens, the atom moves a considerable distance beyond the laser field to the substrate. For a "thick lens," the atom multiply intersects the optical axis of the lens before leaving the laser field. Actually, this case is similar a lens with a refractive index gradient well-known in conventional light optics. Because a lens with small focal distance is required for strong focusing, this means that the thick lens regime, i.e., the regime of atom channeling in the standing wave, is preferable [52].

In a real experiment, the size of the focused spot and, therefore, the size of the nanostructure on the surface depends on a number of additional physical factors. The atomic beam has finite divergence, and atoms of the beam entering the lens of the standing wave at different angles intersect the optical axis at different points. If the transverse coordinate of the atom $|x| > \lambda/8$, the harmonic approximation is not valid and spherical aberrations occur. Chromatic and diffraction aberrations also make a noticeable contribution into the size of the created nanostructure. Of all the factors mentioned above (which influence the focal spot size), the finite divergence of the atomic beam dominates. The influence of this factor is reduced by the transverse collimation of the atomic beam [65]. A spherical aberration results in the pedestal of non-focused atoms; however, its influence on the structure size is insignificant. One of the methods for reducing the pedestal is using an additional mechanical mask with the light wave period situated in such a way that only atoms near the axis of the atom lens ($|x| < \lambda/8$) could pass through it. In the approximation of a thin lens broad velocity, the distribution of the atomic beam results in large chromatic aberrations. However, in the channeling regime (thin lens), even for the velocity distribution width $\Delta v/v \approx 1$, the role of chromatic aberrations is strongly suppressed. There are methods for improving the monochromaticity of atomic beams, such as using supersonic beams or beams cooled in the longitudinal direction. However, using these rather complex methods for focusing atoms does not yield a noticeable gain in the channeling regime.

The small transverse size of an atom lens (~$\lambda/4$) also results in the noticeable influence of diffraction aberrations. For atoms with a velocity of around 200 m/s, the wavelength is about 0.01 nm; this results in the diffraction limit of atom focusing ~$\lambda/40$.

Atoms also experience a transverse velocity and spatial broadening due to processes of the spontaneous re-emission of laser photons. However, this effect can be reduced to an experimentally acceptable value by choosing a sufficiently large frequency detuning.

In addition to the considered effects of the atomic nanostructures broadening due to the atom trajectory deviating from the ideal one, physical and chemical processes on the surface also result in the nanostructure sizes broadening [66, 67]. In [68–70] the role of these effects in nanostructure formation was analyzed.

Nanostructures can be created on the surface using optical methods in two ways: direct deposition nanolithography and resist nanolithography.

Direct Deposition Nanolithography

The method of the direct deposition of laser-focused atomic beams was convincingly demonstrated in experiments [57–63] with a grid of "photonic lenses" formed by standing waves. This configuration of the light field allows one to obtain a large number of periodic nanostructures. Many atoms with corre-

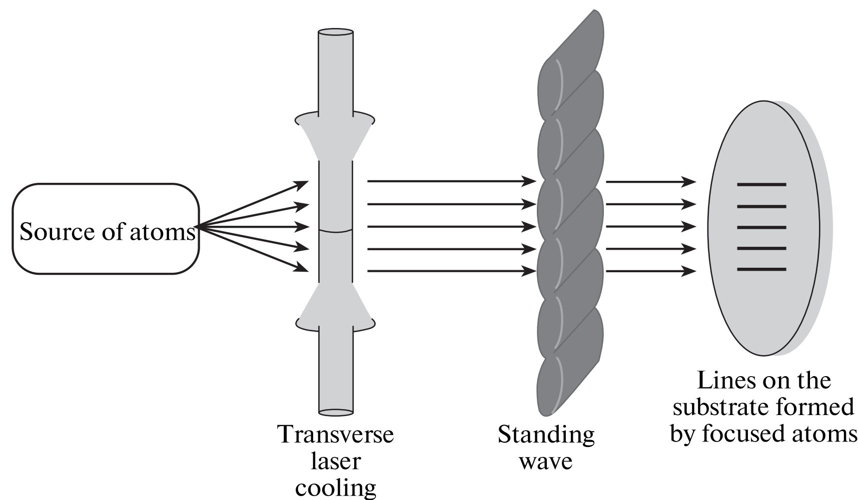

Fig. 8. Schematic diagram of direct deposition nanolithography: two laser beams perform transverse cooling of the atomic beam (collimation). The standing light wave forms cylindrical photonic lenses for atom focusing. Atoms are deposited on the surface in parallel lines due to focusing in the nodes of the standing wave forming the periodic grid of nanostructures.

sponding quantum transitions are potentially applicable for atomic nanofabrication. Quantum transitions should have a wavelength of available continuous lasers.

A typical schematic diagram of experiments applicable for many atoms is shown in Fig. 8. An atomic beam from a thermal source has a too large a divergence for being focused into a nanometer scale even after passing through collimating apertures. The fundamental capability of atom optics (the capability of decreasing the transverse velocity (temperature) of atoms via their transverse cooling (collimation)) is used for reducing the divergence; this capability was first demonstrated for a beam of sodium atoms [65]. This way, the barrier inherent for light optics due to the Helmholtz–Lagrange law is overcome in atom optics. The highly collimated atomic beam then passes through the high-intensity standing wave with the frequency shifted toward the blue region by several hundreds of MHz with respect to the atomic resonance, which pulls atoms into the nodes of the standing wave due to the gradient force, i.e., into the region of minimum potential energy of the atom in the light field. In the case of atoms with the magnetic structure ($J \neq 0$), it is necessary to control the population of magnetic sublevels providing the population of the state $|M| = J$ by optical pumping with circularly polarized light.

The first experiment according to the schematic diagram shown in Fig. 8 was carried out with sodium atoms [57], which were deposited in the form of a grid of nanolines onto the silicon substrate. The grid period was $\lambda/2 = 294.5$ nm, where λ is the wavelength of a dye laser tuned to the transition $3^2S_{1/2}(F = 2) - 3^3P_{3/2}(F = 3)D_2$ of the 589 nm Na line with a saturation intensity of 6.3 mW/cm^2 and a natural width of 10 MHz. The obtained grids are unstable in air and were studied in vacuum using light. The created grid was first registered by the diffraction of laser radiation with a shorter wavelength and then studied using the method of scanning tunnel microscopy. Nanoline grids of Cs atoms were created using the same method [58].

Soon after that, the most convincing experiments on direct deposition nanolithography were carried out with Cr atoms [59, 64]. The advantage of using Cr atoms is that, after nanostructures are manufactured in vacuum, they can be kept in air due to the formation of a very thin oxide film (of around 1 nm). This allows them to be investigated in air using atomic force microscopy. Transverse cooling of the atomic beam using the method of gradient polarization was used in an experiment; this cooling allowed one to obtain a collimated beam with a divergence of order of just 0.1 mrad. Figure 9a shows chromium nanostructures in the form of lines. The width of nanolines at half-maximum was 50 nm, and their height was 28 nm. The height of nanolines depended on the exposure time, which was about 10 min in experiment.

The background coating that occurs is, in particular, due to the isotopes of Cr atoms, which were not in resonance with laser radiation.

If two mutually perpendicular interfering standing waves are used, a 2D grid of “photonic microlenses” can be formed and a 2D nanostructure on the surface can be obtained (Fig. 9b) [72, 79]. This method was also used to obtain nanostructures with the smallest size (just 15 nm) [75].

These pioneering experiments were the basis of subsequent experiments with other field configurations and different atoms and substrates.

A standing light wave is ideal for obtaining 1D-periodic structures (grid of lines) and 2D-periodic structures (a grid of dots). The grid period ($\lambda/2$) can be controlled by changing the wavelength. The period

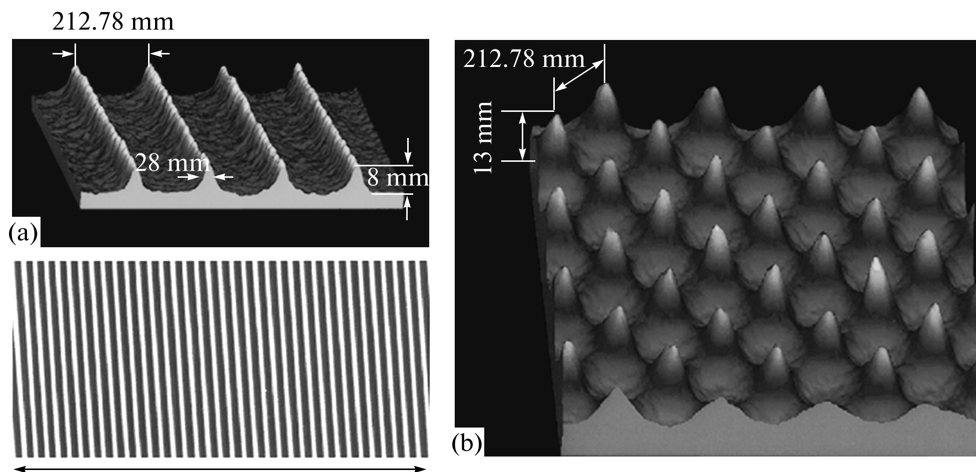

Fig. 9. Image of chromium nanostructures obtained by focusing of (a) 1D and (b) 2D system of photonic lenses. The period of chromium lines and dots is $\lambda/2 = 213$ nm. The images were obtained using atomic force microscopy [72, 79].

$\lambda/8$ can be obtained by changing the polarization in the standing wave (for example, using two counter-directed running waves with orthogonal linear polarization) [71]. For such polarization the optical potential due to the complex interaction of all magnetic sublevels of a Cr atom in the ground state with polarized light changes in space with the period $\lambda/8 = 53.2$ nm. However, this is achieved with a simultaneous reduction in the modulation depth of the obtained grid of atom lines.

The interference of three laser beams intersecting at an angle of 120° can be used. In this case the 2D picture has hexagonal symmetry, which can be additionally controlled by frequency detuning Δ of the field with respect to the atomic resonance in order to pull atoms either to nodes ($\Delta > 0$) or antinodes ($\Delta < 0$) of the interference pattern [76]. In another experiment five laser beams intersecting at an angle of 72° were used to create a decagonal quasiperiodic structure of ^{52}Cr atoms on an area of 0.2×0.2 mm [77].

The complexity of atomic structures depends on the configuration of the light field created by the superposition of many laser beams. Complex configurations can be created by holographic reconstruction of the light field [78]. Using the holographic method is quite promising due to the high angular and spectral selectivity of the holographic "mirror." In particular, holograms for two different wavelengths can be kept, which fundamentally allows one to create a field for two different atoms in one setup with different light field configurations.

It is also important for practical purposes to obtain 3D structures. This field has not been well developed yet; nonetheless, obtaining 3D structures using a combination of Cr atoms and the matrix material MgF_2 was successfully demonstrated [79]. In this experiment ^{52}Cr atoms resonantly interacted with the standing light wave, which provided the modulated (with respect to concentration in the transverse direction) doping of MgF_2 by Cr atoms, while MgF_2 was deposited without any noticeable influence of laser radiation (large laser frequency detuning). It can be expected that a combination of atoms of groups III and V with laser fields at two corresponding resonance frequencies would allow heterostructures modulated in the transverse direction to be obtained, which is of interest for metamaterial design.

Next was the beam of magnetic Fe atoms, which was more complex for the experiment [80, 81]. Radiation with a shorter wavelength ($\lambda = 372$ nm) is necessary for resonant excitation. Moreover, it is difficult to achieve laser cooling for such atoms, because they do not possess an ideally closed cyclic transition. With a probability of 1/243, the excited Fe atom returns to the metastable state rather than the initial state and loses resonance with radiation. Nonetheless, grids of nanolines with widths of 50 nm and regular periods of 186 nm were successfully obtained in the experiments. Such ultraregular ferromagnetic nanogrids can be used in experiments on spintronics and experiments with nanomagnetics. Using lasers with shorter wavelengths would allow one to perform experiments on nanofabrication with other magnetic atoms (^{58}Ni 323.4 nm, ^{59}Co 240.5 nm).

Successful experiments were also performed with atoms of the rare-earth element Yb [82]. Prospects of experiments with potentially important ^{27}Al (309.4 nm), ^{69}Ga (294.4 nm), ^{115,113}In (325.7 nm) atoms, which require continuous lasers in a poorly mastered UV region, were considered [78].

So far, only the several simplest configurations of the type of standing light waves and their combinations were used for nanofabrication; therefore, a broad field is left for future studies.

Resist Nanolithography

Resist is used in conventional lithography, specifically, a photoresist sensitive to UV (or VUV) radiation. This method can be used for nanolithography with a light mask. The light mask creates a spatially inhomogeneous distribution of excited (metastable) or chemically active atoms which modify the resist. Further etching of the exposed resist is performed using standard lithography methods. For this approach in nanofabrication, substrates of any materials which can be etched, including such important magnetic materials as Ni and Fe, are applicable. In atom optics, methods of resist nanofabrication using excited metastable atoms of noble gases (He*, Ne*, and Ar*) and chemically active alkali atoms (Na, are Cs) were demonstrated.

Metastable Atoms of Noble Gases

The first resist used in nanolithography was a self-organized monolayer (with a thickness of 1.5 nm) of dodecane ethiole on a gold-covered substrate [71]. Molecules of a highly ordered monolayer form the hydrophobic surface, which protects the substrate from chemical etching in a water solution. Metastable atoms with high internal energies (up to 20 eV for He*) or chemically active atoms destroy the local ordering of organic molecules and provide subsequent local etching. This technology, based on the light mask of atom excitation, was demonstrated for the standing wave [72]. Nanostructures 65 nm in size, determined by the wave nature of atoms, were obtained in the experiments [73].

Instead of the local destruction of the resist film of self-organized molecules, the destruction in the film of background oil molecules on the resist surface can be used; these molecules are deposited on the substrate when the chamber is pumped out using an oil pump. The spatial structure of the local destruction of this background film that is created can be transferred to the substrate for subsequent etching using an ion beam [74].

Chemically active atoms of alkali elements. Alkali atoms can be focused by the gradient force of the light field of both continuous and pulsed lasers and modify surfaces on a nanometer scale using their high chemical activity.

NEAR-FIELD ATOM MICROLENSES

Atom optics based on running and standing laser fields has a number of constraints of both fundamental and technical characters which occur due to the spatial "non-localization" of laser fields. The "non-localization" of the laser field results in the "non-localization" of atom optics elements. The consequence of this is the imperfection of atom optics elements: the aberrations of atom lenses, low diffraction efficiency of atom waves, constraints on the contrast of interference bands in atom interferometers, and so on.

It is clear from general physical considerations that using spatially localized atom–field interaction potentials is preferable for constructing atom optics elements, in particular, atom lenses. Three types of sufficiently well spatially localized laser fields are currently known: (a) the surface light wave, which is formed in the case of total internal light reflection (1D light localization); (b) the light field formed at light diffraction on structures smaller than the light wavelength (2D light localization); and (c) the light field localized in partially open waveguides (the "photon dot" and "photon hole" (3D light localization)). The two latter types of laser nanofields are used in atom lithography.

BETHE HOLE-BASED ATOM LENS

The most well known example of 2D light localization is based on the application of the Bethe hole, a hole in a thin conducting screen with a diameter smaller than the wavelength of incident radiation [84–87]. The possibility of using such a nanolocalized field for the problems of focusing atomic beams was studied in [88–91]. It was shown [89–91] that a set of near-field microlenses can be used for creating micro- and nanostructures on the surfaces.

The idea of a single near-field atom lens based on Bethe hole is shown in Fig. 10. Laser light illuminates the conducting screen with a hole whose diameter is smaller than the light wavelength. The field on the upper side of the screen consists of the running wave and the near-field component. The latter has the following specific features important for creation of an atom lens: (1) the value of the near-field component in the neighborhood of the hole has an order of magnitude of the incident field; (2) the near-field component damps beyond the screen on a characteristic length of order of the hole size; and (3) the near-field component possesses axial symmetry in the plane parallel to the screen, and its value changes approximately proportionally to the squared distance from the hole axis. The exact formal solution to the problem of the diffraction of a plane wave on a circular aperture in an infinitely thin metal plane was obtained in a number of papers [84–87]. Figure 10a shows the near-field light distribution (red curves).

An analysis of near-field atom focusing showed [89–91] that effective focusing can be achieved for a relatively slow atomic beam. If the velocity of atoms is high, the small interaction time limits the focusing capabilities of the lens, while, for the low velocity, the diffraction limits the focal size of the atomic beam. The size of the minimal focal spot is determined by a number of factors, including: (a) spherical aberrations, (b) chromatic aberrations, (c) the diffraction of atoms on the aperture, (d) the finite divergence of the incident atomic beam, (e) inter-atomic interaction when there is sufficiently high density, and (f) spontaneous emission. Taking into account the above factors,

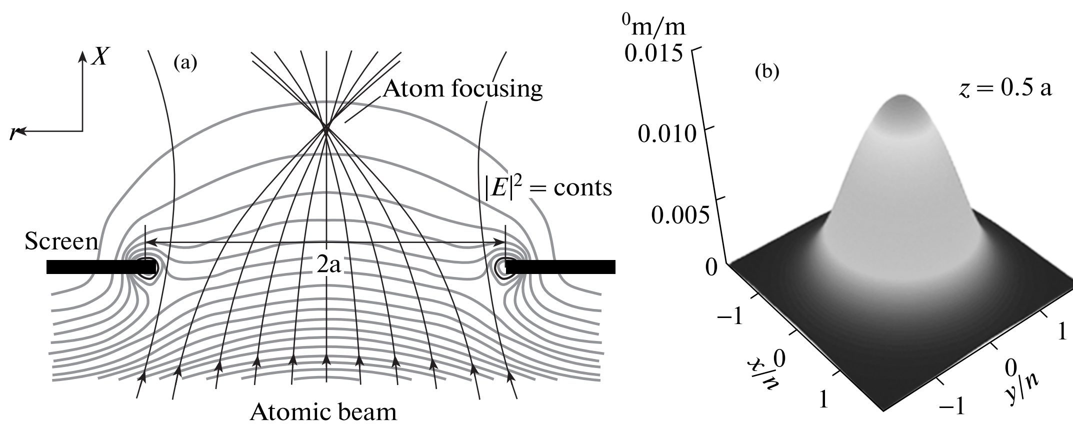

Fig. 10. (a) Idea of a single near-field atom lens; (b) near-zone light field distribution.

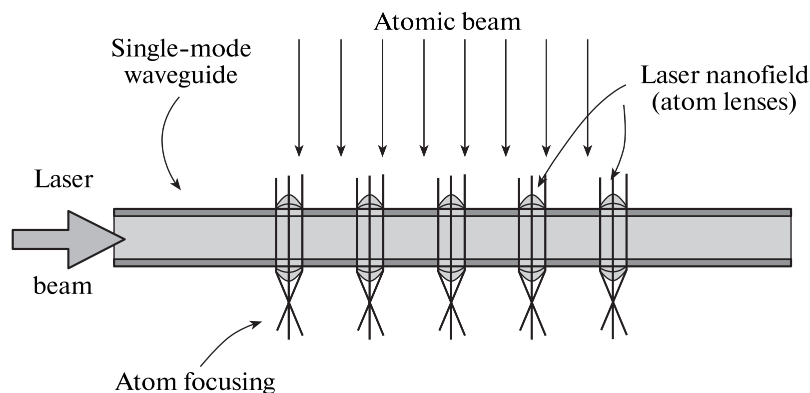

Fig. 11. Schematic diagram of obtaining spatially localized light nanofield inside a plane waveguide near nanoholes and atom focusing by such nanofields.

the focal size of the focused atomic beam makes 0.1 of the optical wavelength.

PHOTON DOT- AND PHOTON HOLE-BASED ATOM LENS

The most important disadvantage of the field localized near a single hole as an atom microlens is the fact that this field is inseparably connected with the field of the accompanying standing wave. If the atom moves in this region, spontaneous decay is possible; in many cases this decay is undesirable for atom lithography. New types of spatially localized laser fields with characteristic spatial sizes in a nanometer scale which were free from the above disadvantage were studied [90–92].

The schematic diagram of obtaining such spatially localized light nanofield is shown in Fig. 11. Two plane conducting screens with a distance between the planes on the of order or smaller than the light wavelength form a plane 2D waveguide for laser radiation input into it. It is known that, for a waveguide consisting of two parallel ideally conducting planes, there are solutions to Maxwell equations which admit radiation propagation in the waveguide for an arbitrarily small thickness d, including a thickness much smaller than the radiation wavelength.

If two small coaxial holes with the radius a are formed in a conducting screen and the hole diameters are much smaller than the input radiation wavelength ($a \ll \lambda$), the radiation practically does not leave these holes; however, near each hole the field inside and beyond the waveguide is strongly modified. Near the holes the field decreases in the region with the characteristic spatial size of order of the hole diameter, i.e., considerably smaller than the radiation wavelength. The volume of this region is $V \ll \lambda^3$. The field modification near the holes depends on the polarization of the laser field inside the waveguide. The energy density distribution for the radiation with the electric field vector perpendicular to the waveguide plane is shown in Fig. 12. Such a modified field distribution near the holes was called the "photon hole" [90]. It can be seen that the characteristic size of the photon hole is determined by the hole size and the waveguide thickness.

Figure 13 shows the field intensity distribution near the holes of the plane waveguide and inside the

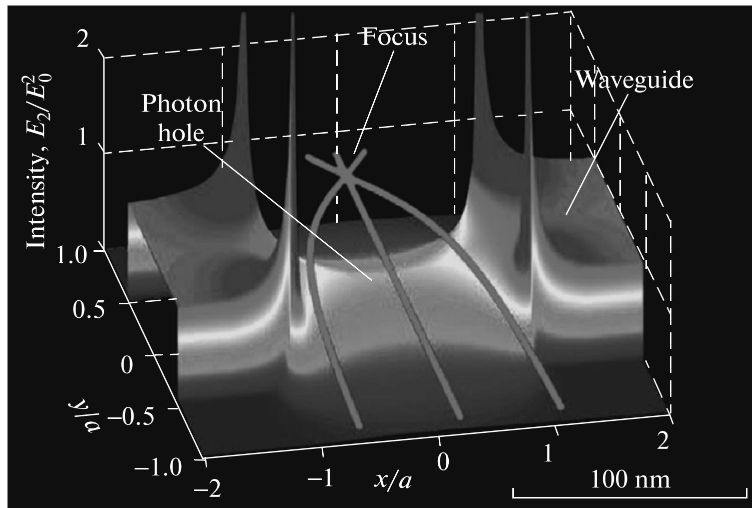

Fig. 12. Field intensity distribution near the hole in the plane waveguide and inside the plane waveguide for the case when the electric field vector of laser radiation is perpendicular to the waveguide plane: "photon hole." Trajectories of atoms focused by the nanofield are shown schematically.

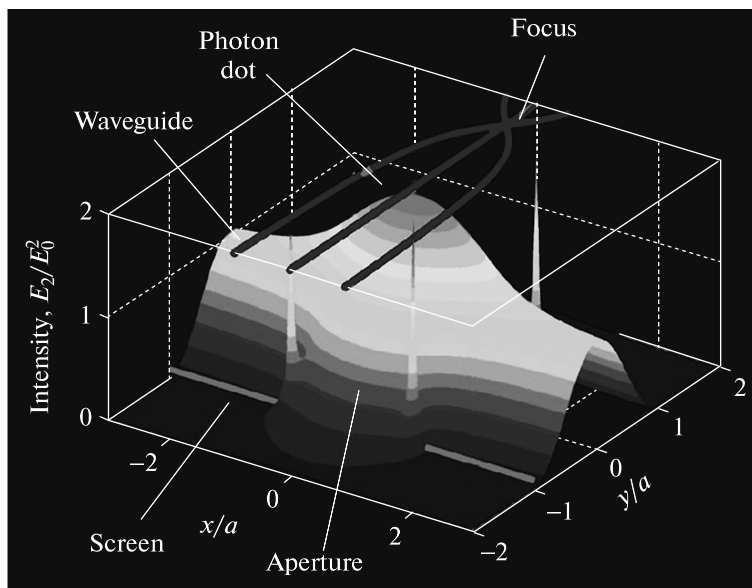

Fig. 13. Field intensity distribution near the hole in the plane waveguide and inside the plane waveguide for the case when the electric field vector of laser radiation is parallel to the waveguide plane: "photon dot." Trajectories of atoms focused by the nanofield are shown schematically.

waveguide when the electric field vector of laser radiation is parallel to the waveguide plane, the waveguide thickness is equal to one half of the wavelength, and the hole radius $a = \lambda/2$. It can be seen from the figure that the field drops rather fast beyond the waveguide in a direction perpendicular to the waveguide plane and has a maximum in the middle of the waveguide; i.e., the "photon dot" is formed. The characteristic volume of this photon dot is also smaller than λ^3. Sharp peaks of field intensity near the aperture edge occur due to the assumption of the infinite conductivity of the waveguide walls. The field intensity maximum is two times larger than the maximum in the case of one hole, which is due to the structural interference of the fields scattered by the holes. This circumstance provides the application of lower laser fields, unlike the case of a single hole.

The photon dot and photon hole can be used for focusing atomic beams by the gradient force which is proportional to the electric field intensity [90, 92].

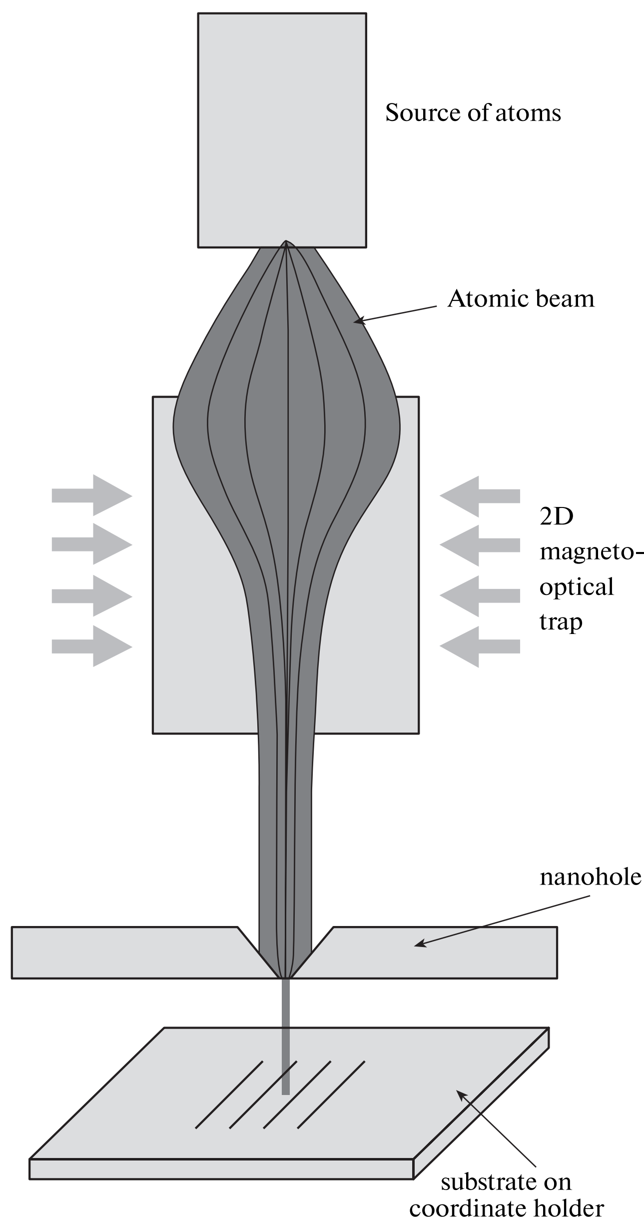

Fig. 14. Schematic diagram of atom optical nanopen for drawing atomic structures.

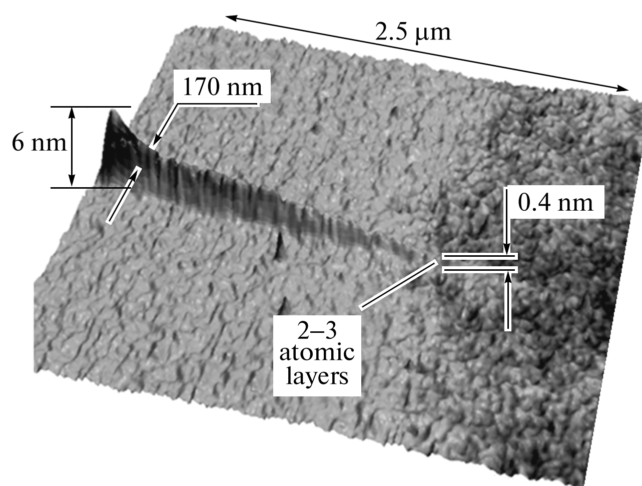

Fig. 15. Nanostructure of Cr atoms in the form of a band with variable height created using the atom optical nanopen.

ATOM NANOPEN LITHOGRAPHY

The transportation of atoms in a hollow fiber waveguide [93] and their nanoaperture near-field focusing [88] underlies the idea of the atom optical "pen" shown in Fig. 14. A hollow fiber or screen with a nanoaperture can be controlled in the transverse direction using a cantilever; this was successfully used for nanofabrication using the direct deposition method [94]. The atomic pen can potentially be a universal method of "nano-drawing" [94, 96], although there are obvious constraints on the performance of such nanofabrication due to slow scanning. Laser cooling, collimation, and concentration of the atomic beam can be achieved in a narrowing ("horn"-type) hollow optical waveguide [95], which considerably increases the atomic pen efficiency. Figure 15 shows one of the nanostructures from Cr atoms created using the atom nanopen [96]. The width of the formed nanostructures at half-maximum is 170 nm.

In principle, scanning the atomic De Broglie wave by laser light can be done along with mechanical nanoscanning. Such an atomic scanner was experimentally demonstrated [97].

The advantages of nanolithography using atom nanopen were used in [98] for the creation of ultrasensitive surface mass detectors. More than 2000 mechanical microresonators monolithically integrated into CMOS-type electric circuit were created from Al atoms using the atom nanopen on a silicon plate with a diameter of 10 cm (Fig. 16). The minimal size of a microresonator element was about 200 nm. This is an example of successfully combining two nanolithographic technologies: photolithography for the creation of a CMOS circuit and atom nanopen for the creation of microresonators.

ATOM PINHOLE CAMERA

In spite of the presence of multiple proposals for focusing atomic beams and multiple experimental atom lenses being achieved, the problem regarding the construction of nanoobjects of an arbitrary shape has not yet been solved. The main complexity is the creation of atom–electromagnetic field interaction potential with properties close to those of the "ideal" lens for atoms (with minimal chromatic aberration and compensated astigmatism, which provides atomic beam focusing into a diffractionally limited spot).

In [96] a new approach to constructing object images in atom optics based on the idea of the pinhole

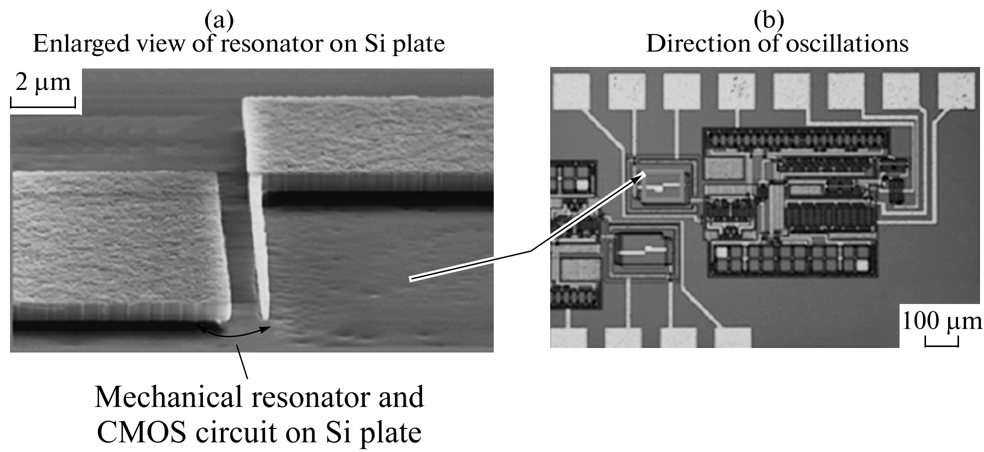

Fig. 16.

camera, which is well-known in light optics, was first experimentally achieved. The pinhole camera is also used in modern experimental physics when it is difficult to create a focusing potential for a certain type of particles [99].

It is well known from light optics that a pinhole camera is capable of producing a high-quality image of an object. The two basic questions arising when consideration a particular type of pinhole camera are as follows: (1) what is the optimal hole size for achieving maximal resolution? and (2) what is the expected resolution in this case? In order to answer these questions, it is necessary to perform a detailed study based on the diffraction theory. However, the basic idea of the pinhole camera optics can be obtained from qualitative physical considerations. It is clear that a large diaphragm for the given distance to the image plane does not provide a high-quality image. At the same time, if the hole is too small, the wave diffraction also prevents the image from being constructed. The standard approach upon obtaining the image using a pinhole camera is to construct the image of a point object at infinity. In this case the plane wave is incident on the screen with the hole of the radius S, and the spot with the radius r is formed at the distance f (focal distance of the pinhole camera). The best pinhole camera is one that produces the smallest spot. If the hole in the screen is large, the spot represents the geometrical shadow of the hole and the image radius is equal to the hole radius. If the hole decreases, the image spot formation should be described by a Fresnel or Fraunhofer diffraction. For a circular hole, the spot radius in this case is $r \approx 0.61\lambda(f/s)$. Thus, the spot radius is approximately equal to the sum of the geometric shadow and the diffraction spot,

$$R = S + 0{,}61\lambda(f/s). \tag{14}$$

The smallest size is achieved when geometric optics and the diffraction theory yield the same results, i.e., if the following condition is satisfied: $S^2 \approx 0.61\lambda f$. The consideration based on the diffraction theory demonstrates that the pinhole camera resolution can be even better than the geometrical one [100]. An exact calculation demonstrates that the effective wave concentration at the optimal distance is smaller than the hole diameter by a factor of 3, and the optimal hole is larger than half of the Fresnel zone and smaller than the total first zone.

An atom pinhole camera possesses a chromatic aberration. This follows from the dependence of the optimal focal distance on the wavelength, $f_{\text{opt}} \approx s^2/\lambda_{bB}$. In particle optics lenses based on electromagnetic interaction potentials, there is a quadratic dependence of the chromatic aberration on the particle velocity. In the pinhole camera, because of the linear dependence of the optimal focal distance on the atom velocity, the chromatic aberration is linear with respect to the atom velocity; i.e., this type of aberration is less significant. The pinhole camera is free from linear distortion aberrations and possesses insignificant astigmatism.

The earlier consideration assumed that, in a pinhole camera, the screen with the hole is infinitely thin. In a real experiment, the screen thickness is finite and, for a sufficiently small hole size, the action of van der Waals forces begins to manifest itself. An analysis shows that van der Waals forces impose additional constraints on the minimal nanohole size $a_{\min}$,

$$s \gg a_{\min} = \sqrt[5]{\frac{12C_3dl}{E_k}}, \tag{15}$$

where C_3 is the van der Waals coefficient, d is the screen thickness, and E_k is the kinetic energy of atoms. For example, for Cs atoms and the silicon screen with a thickness of 50 nm, the minimal hole radius is $a_{\min} = 5.8$ nm.

It follows from this examination of the pinhole camera that achieving this requires the application of a nanometer hole diameter in the nanometer-thick screen. The atom pinhole camera built in [101] was

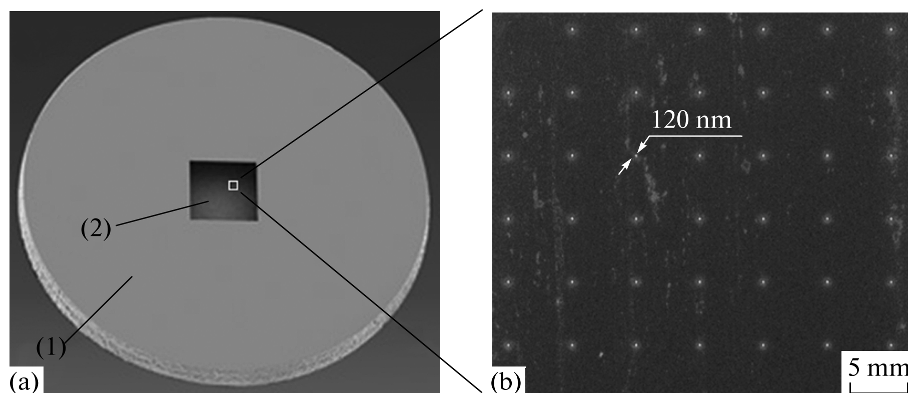

Fig. 17. (a) Photo of the membrane with nanoholes for atom pinhole camera: (1) membrane holder in the form of a disc with a diameter of 3 mm and a thickness of 200 μm with a 0.5 × 0.5-mm window at the center; (2) membrane from Si_3N_4 with a thickness of 50 nm. The white square marks the field with nanoholes [101]. (b) Electron image of part of the membrane with nanoholes 120 nm in diameter.

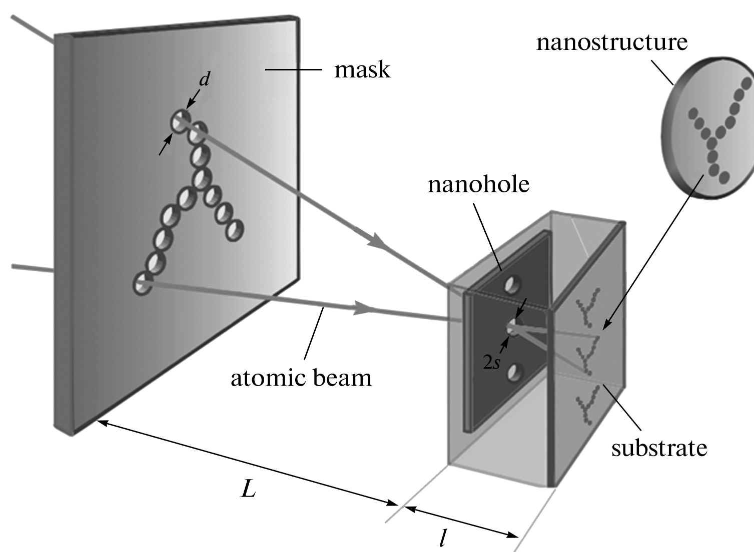

Fig. 18. Schematic diagram of an atom pinhole camera. Atoms passed through the holes in the mask form (similarly to light optics) a "glowing object" with the given geometry. An atom nanostructure whose shape is a reduced copy of the mask is created on the substrate using the nanohole.

constructed using nanometer-thick membranes in which nanoholes were manufactured using a focused ion beam [103]. This method makes it possible to create nanoholes with a diameter of up to several nanometers. For producing nanoholes for pinhole camera, membranes manufactured by Ted Pella Inc. were used. The membranes were made up of an ultrathin film from silicon nitride with a thickness of 50 nm situated on a silicon plate with a diameter of 3 mm and a thickness of 0.2 mm. Figure 17 shows the membrane image (obtained using a scanning electron microscope) (a) and nanoholes (b) in this membrane. The nanohole diameter is equal to $d = 120$ nm.

The schematic diagram of the pinhole camera achieved in experiment [101] is shown in Fig. 18. It includes the atomic beam, the mask, the membrane with nanoholes, and the substrate on which nanostructures were created. Atoms that passed through the hole in the mask form, similarly to optics, the "glowing object" with the given geometry. The parameters of the pinhole camera were chosen from the considerations of obtaining maximal resolution and the possibility of constructing of a large array of nanostructures on the surface. If thermal atomic beams with typical de Broglie wavelengths of around 10^{-2} nm and a nanohole with a diameter of 20 nm are used, the optimal focal distance is $f_{opt} \approx 10$–20 μm. This determined the choice of the distance between the nanohole and the substrate on which nanostructures were created ($l = f_{opt}$). For the given value of l, the distance from the

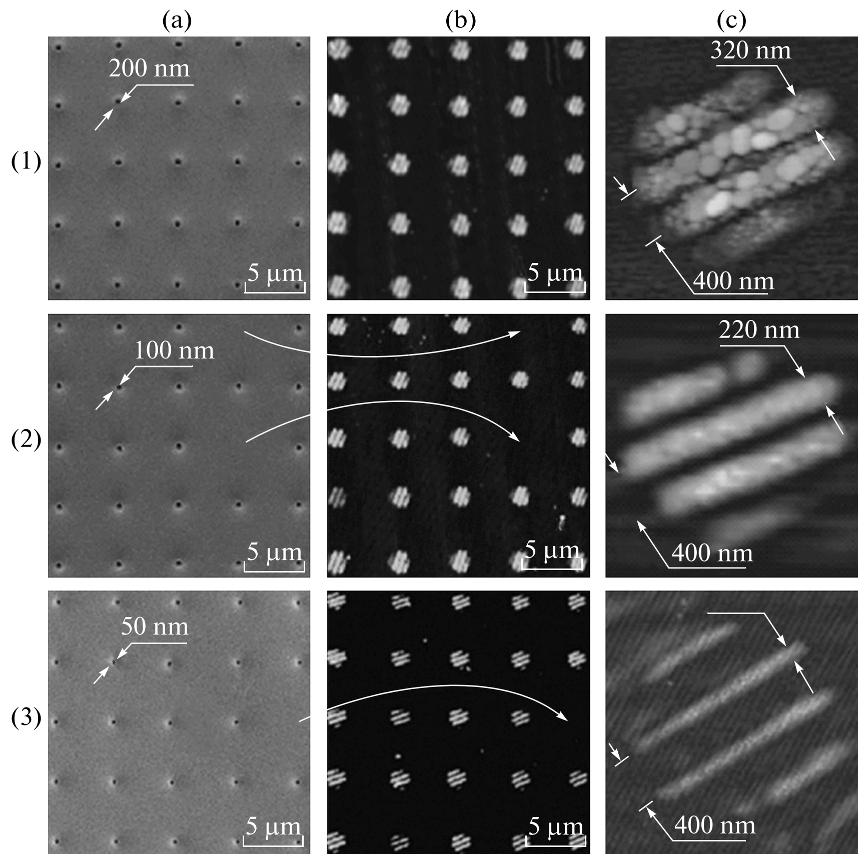

Fig. 19. Atom nanolithography of identical nanostructures using an atom pinhole camera. (a) Left column shows electron images of membranes with nanoholes with diameters of (1) 200 nm, (2) 100 nm, and (3) 50 nm. (b) Middle column shows images of created nanostructures from In atoms on the silicon surface. (c) Right column shows the enlarged images of one nanostructure from the middle column [101].

nanohole to the mask determines the "reduction force" of the atom pinhole camera $N = L/l$ and, therefore, the mask size.

The fundamental difference between the atom pinhole camera and the optical pinhole camera is the constraint on the maximal atomic density available in experiment. It is well known that it does not exceed 10^{10} atoms/cm^3 for effusion atomic beams. This constraint, in turn, results in the constraints on the formation time of nanostructures and their height.

The above considerations show that the optimal distance from the nanohole to the mask is in the range $L = 1$–10 cm. The reduction force of the pinhole camera $N = L/l$ in this case is 10^3–10^4. In this pinhole camera geometry, the characteristic size of the mask is in the micrometer range and the characteristic size of the created structures is in the nanometer range; i.e., the atom pinhole camera provides the transformation of micro-objects into nano-objects. Another important consequence of the "dimensional geometry" of the atom pinhole camera is the possibility of using a large number of nanoholes (instead of only one) in one device. In this case each nanohole creates its image which does not intersect neighboring images; i.e., it is possible to achieve a "parallel atom pinhole camera." A parallel atom pinhole camera creates broad opportunities for the simultaneous creation of a large number of identical nanostructures. It should be noted that, even for a considerable number of nanoholes (up to 10^6), aberrations of inclined beams (which begin to manifest themselves for edge nanoholes) do not strongly limit the resolution of the parallel atom pinhole camera.

A parallel atom pinhole camera with above parameters [101] was used to create nanostructures from In, Cr, and Ag atoms on a silicon surface. The time that a series of nanostructures was created on one substrate was determined by the atomic beam intensity and the required value of the nanostructure height. The characteristic exposure time in the experiment made $t \sim 10$ min for nanostructures with a height of $h \sim 25$ nm.

Figure 19 shows the images of nanostructures created using the parallel atom pinhole camera. Nanostructures were visualized using an atomic force microscope. The mask was a thin metal screen (in which the grid consisted of slits with a width of 250 μm, a length of 5 mm, and a period of 1 mm) was manufactured by laser cutting. Three different mem-

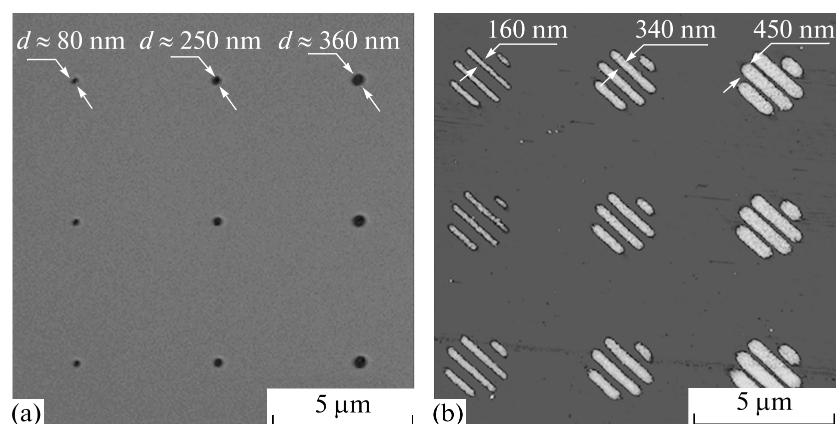

Fig. 20. Influence of the nanohole size on the resolution of the atom pinhole camera. (a) Electron image of the membrane with nanoholes of different diameters: d = 80, 250, and 360 nm; (b) images of nanostructures created from In atoms on the silicon surface using nanoholes of membrane (a) [101].

branes with different nanohole diameters were used: $d_1 = 200$ nm, $d_2 = 100$ nm, and $d_3 = 50$ nm (column (a) in Fig. 19). The images of nanostructures obtained using these membranes are shown in columns (b) and (c) in Fig. 19. Column (b) shows the survey images of a large number of nanostructures. Column (c) shows the detailed images of one of the nanostructures from column (b). It can be seen in Fig.19 that the position of nanostructures on the silicon substrate repeats the geometry of nanoholes in the membrane. In order to underline this fact, in membrane no. 1 (Fig. 19.1a) nanoholes were situated in regular staggered order 5 × 5. As a result, nanostructures obtained using membrane no. 1 are also situated in regular staggered order. In membranes nos. 2 (Fig. 19.2a) and 3 (Fig. 19.3a), part of the nanoholes are absent. The position of nanostructures on substrates nos. 2 and 3 completely corresponds to the position of nanoholes in the applied membranes: the absence of nanoholes results in an absence of nanostructures (shown by arrows in the figure).

The presented nanostructure images demonstrate that their shape repeats the mask topology: an individual nanostructure consists of parallel bands formed by In atoms at the same distance of ≈400 nm from each other.

The influence of the diameter of the applied nanohole on the resolution of the atom pinhole camera is shown in Fig. 20; in this figure, the results of nanolithography with holes of a different diameter (Fig. 20a) are shown. It can be seen from the figure that the position of nanostructures on the substrate corresponds to the position of nanoholes in the membrane of the pinhole camera. Nanostructures created using holes with different diameters differ in band width Δ and nanostructure height h. The dependence of the band width on the nanohole diameter agrees with the optics of the pinhole camera, the corresponding band widths are $\Delta_1 \approx 160$ nm, $\Delta_2 \approx 340$ nm, and $\Delta_3 \approx 450$ nm. The nanostructure heights are $h_1 \approx 9$ nm for holes with the diameter $d_1 = 80$ nm, $h_2 \approx 12$ nm for the hole with the diameter $d_2 = 250$ nm, and $h_3 \approx 17$ nm for the hole with the diameter $d_3 = 360$ nm. The nanostructure height, depending on the nanohole diameter of the atom pinhole camera, is determined by three processes: (1) the decrease in the atomic beam intensity near the substrate surface with the decreasing nanohole diameter; (2) the decrease in the beam intensity due to the adsorption of part of the atoms on the walls of the nanohole channel in the membrane, resulting in a reduced size after some time; (3) the dependence of the atom pinhole camera resolution on van der Waals forces.

To investigating the limiting parameters of nanolithography using the atom pinhole camera, measurements concerning the creation of nanostructures using a nanohole with a diameter of 20 nm were performed. In this case the pinhole camera operation conditions in the wave optics regime are achieved. The influence that atomic de Broglie wave diffraction has on the nanohole parameters and the van der Waals forces become important. A mask consisting of slits with different widths in a metal foil (Fig. 21a) was used in the experiment. The nanostructure obtained in this geometry of the atom pinhole camera is shown in Fig. 21b. The minimal element size in the created nanostructure is equal to 30 nm; it is formed by atoms that passed through the 40-μm-wide slit in the mask. The height of this nanostructure element does not exceed 0.6 nm.

The results obtained using the parallel atom pinhole camera demonstrate the possibility of creating nanostructures which can be identical or differ with respect to geometric dimensions depending on the type of the applied membrane. The shape and geometric dimensions of nanostructures are determined by the topology of the applied mask and the size of nanoholes in the membrane. In this case it is possible to control not only the planar dimensions of nanostructure elements, but also their heights. This circum-

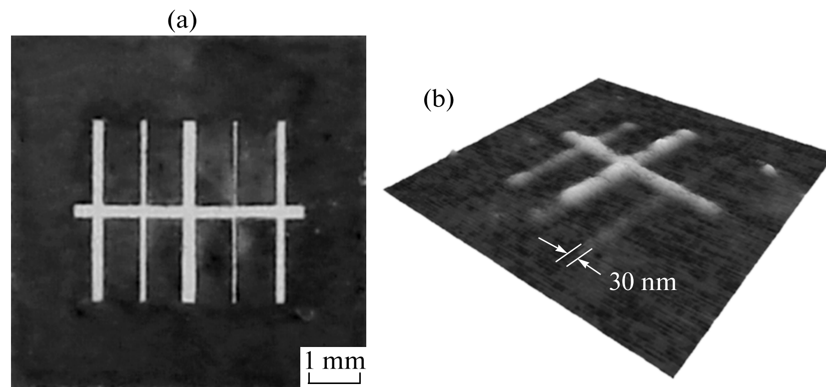

Fig. 21. Creation of nanostructures with a minimal element size of 30 nm: (a) photo of the applied mask and (b) image of the nanostructure from In atoms on the silicon surface [101].

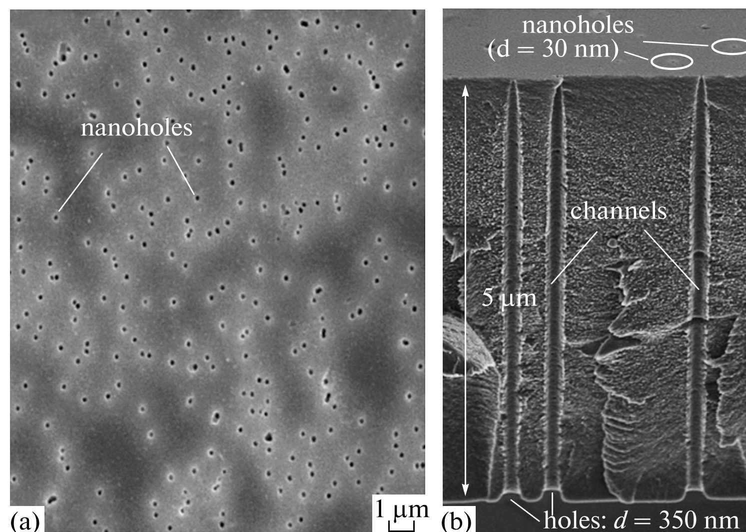

Fig. 22. Image of a segment of track membrane used for atom nanolithography in scanning electron microscope [102]: (a) view from above and (b) transverse cleavage of the membrane.

stance opens capabilities for creating nanostructures with complex 3D geometry, because the nanostructure shape is determined by the geometry of holes forming the mask and the height of separate nanostructure elements is determined by the diameter of these holes.

The atom pinhole camera was used to demonstrate the possibility of mass producing identical nanostructures with about 1 million nanostructures per one deposition [96]. In [96] the pinhole camera was created using nanoholes manufactured in track membranes. In track membranes the area with nanoholes can occupy up to several square meters for a rather high hole density (up to 3×10^7 cm^{-2}). This allows one to create identical nanostructures on substrates with large surface areas. In [96] track membranes were manufactured from 5-μm-thick polyethyleneterephthalate film irradiated by a beam of accelerated krypton ions with an energy of 253 MeV. Each ion passing through the film leaves a deformation track caused by the violation of the chemical bonds between atoms of the film material. Then the film was exposed to ultraviolet radiation from one side only, and after that it was chemically etched. The use of the surface-active substance made it possible to obtain nanopores with sharp size reduction toward the surface that was not exposed to UV radiation [102]. This approach provides the formation of through channels with a minimal input hole diameter of up to 50 nm in the film (Fig. 22). The obtained output channel hole has a characteristic diameter of up to several microns, which allows one to decrease the influence of van der Waals forces on atom trajectories in the atom pinhole camera. Figure 23 shows the image of one of 10 million nanostructures on the glass surface created from Cr atoms using the pinhole camera based on track membranes and the mask in the form of a cross.

The method for creating nanostructures using the atom pinhole camera is related to the category of nan-

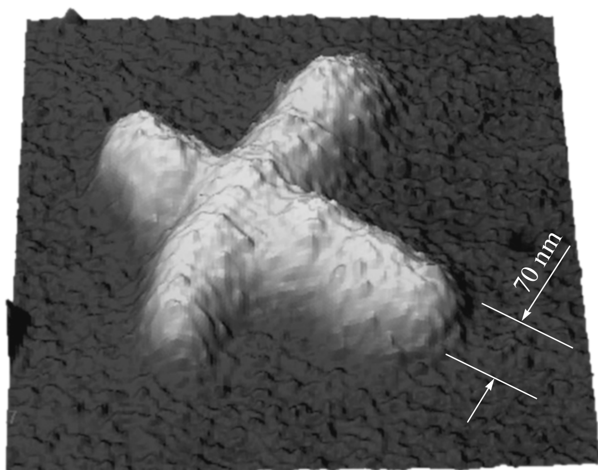

Fig. 23. Atomic force microscopy of images of one nanostructure (out of several million) from Cr atoms created on the glass surface. Nanostructures were created using the pinhole camera based on track membranes. A mask in the form of a cross was used [96].

olithography methods using masks. In conventional nanolithography methods that use masks, mask elements should have dimensions in the nanometer range. Due to the nanometer mask scale, their manufacture is a complex technical task. One of the advantages of using an atom pinhole camera for nanolithography is its capability of creating images with very large object size reduction (up to 10 thousand times). This makes it possible to use masks in the micrometer range whose production does not present technological difficulties.

Note the other important advantages of nanolithography: (1) this method provides the creation of nanostructures with characteristic sizes of up to 20 nm; (2) nanostructures can have an arbitrary predetermined shape; (3) the size and shape of nanostructures is determined by easily controllable parameters; (4) it is possible to create a large number of identical nanostructures; (5) a wide choice of nanostructure material is available (atoms, molecules, clusters, and biomolecules); (6) this method does not require the use of chemically selective etching; and (7) in the course of creating nanostructures, the substrate surface is not destroyed.

CONCLUSIONS

Up until now, important fundamental studies in the field of manipulation with free neutral atoms using the methods of atom optics have been performed and methods for constructing basic optical elements on matter structures, static electric and magnetic fields, and laser fields have been developed. Based on these methods, approaches providing the high-precision control of the motion of atoms as they approach the surface have been developed; this resulted in the development of one practically important direction for atom optics: atom nanolithography.

Currently, optical lithography using far VUV radiation, lithography with electron and ion beams, and X-rays is being developed. These methods are capable of creating nanostructures with a resolution up to several nm. At the same time, a wide search for alternative methods, such as the scanning nanoprobe method, the "imprinting" method, and nanostructure "self-assembly" is being carried out. It is among these alternative future nanolithography methods that the approaches discussed in this survey should be considered.

REFERENCES

1. K. E. Drexler, *Nanosystems: Molecular Machinery, Manufacturing, and Computation* (Wiley, New York, 1992).
2. C. A. Mack, *Fundamental Principles of Optical Lithography: The Science of Microfabrication* (John Wiley & Sons, London, 2007).
3. Y. Chen and A. Pepin, "Nanofabrication: Conventional and Nonconventional Methods," Electrophoresis **22**, 187–207 (2001).
4. D. G. Bucknall, *Nano lithography and Patterning Techniques in Microelectronics* (Woodhead, Cambridge, 2005).
5. J. Orloff, L. Swanson, and M. Utlaut, *High-Resolution Focused Ion Beams: FIB and Applications* (Kluwer, New York, 2002).
6. A. A. Tseng, Kuan Chen, C. D. Chen, and K. J. Ma, "Electron Beam Lithography in Nanoscale Fabrication: Recent Development," IEEE Trans. Electron. Packag. Manuf. **26**, 141 (2003).
7. G. J. Leggett, "Scanning Near-Field Photolithography—Surface Photochemistry with Nanoscale Spatial Resolution," Chem. Soc. Rev. **35**, 1150 (2006).
8. M. Behl, J. Seekamp, S. Zankovych, C. M. S. Torres, R. Zentel, and J. Alpelto, "Towards Plastic Electronics: Patterning Semiconducting Polymers by Nanoimprint Lithography," Adv. Mater. **14**, 588 (2002).
9. B. D. Terris and T. Thomson, "Nanofabricated and Self-Assembled Magnetic Structures as Data Storage Media," J. Phys. D: Appl. Phys. **38**, R199 (2005).
10. V. I. Balykin and V. S. Letokhov, "Laser Optics of Neutral Atomic Beams," Phys. Today **42** (4), 23 (1989).
11. V. I. Balykin and V. S. Letokhov, "The Laser Optics of Neutral Atomic Beams," Usp. Fiz. Nauk **160** (1), 141 (1990) [Sov. Phys.—Usp. **33** (1), 79 (1990)].
12. V. I. Balykin and V. S. Letokhov, *Atom Optics with Laser Light* (Harwood, Chur, Australia, 1995).
13. P. Meystre *Atom Optics* (Springer, New York, 2001).
14. V. I. Balykin, V. S. Letokhov, and V. G. Minogin, "Cooling Atoms by Means of Laser Radiation Pressure," Usp. Fiz. Nauk **147** (9), 117–177 (1985) [Sov. Phys.—Usp. **28** (9), 803 (1985)].
15. V. G. Minogin and V. S. Letokhov, *The Pressure of Laser Radiation on Atoms* (Nauka, Moscow, 1986) [in Russian].

16. A. P. Kazantsev, G. I. Surdutovich, and V. P. Yakovlev, *The Mechanical Action of Light on Atoms* (Nauka, Moscow, 1991) [in Russian].

17. H. J. Metcalf and P. Straten, *Laser Cooling and Trapping* (Springer, New York, 1999).

18. V. I. Balykin, V. G. Minogin, and V. S. Letokhov, "Electromagnetic Trapping of Cold Atoms," Rep. Prog. Phys. **63**, 1429 (2000).

19. V. I. Balykin, V. V. Klimov, and V. S. Letokhov, "Atom Nano-Optics," Opt. Photonics News **16**, 33–36 (2005).

20. V. I. Balykin, V. V. Klimov, and V. S. Letokhov, *Atom Nano-Optics: Handbook of Theoretical and Computational Nanotechnology*, Ed. by M. Rieth and W. Schommers (Elsevier, Amsterdam, 2006), Vol. 7.

21. E. A. Cornell and C. E. Wieman, "Nobel Lectures: Bose–Einstein Condensation in a Dilute Gas: The First 70 Years and Some Recent Experiments," Rev. Mod. Phys. **74**, 875–893 (2002); W. Ketterle, "Nobel Lectures: When Atoms Behave as Waves: Bose–Einstein Condensation and the Atom Laser," Rev. Mod. Phys **74**, 1131–1151 (2002).

22. N. F. Ramsey, *Molecular Beams* (Clarendon, Oxford, 1956).

23. F. Knauer and O. Stern, "Über die Reflexion von Molekularstrahlen," Z. Phys. **53**, 779–791 (1929).

24. L. Estermann and O. Stern, "Beugung von Molekularstrahlen," Z. Phys. **61**, 95–125 (1930).

25. V. U. Nayak, D. O. Edwards, and N. Masuhara, "Scattering of ^{4}He Atoms Grazing the Liquid–^{4}He Surface," Phys. Rev. Lett. **50**, 990 (1983).

26. A. Anderson, S. Haroche, E. A. Hinds, W. Jhe, D. Meschede, and L. Moi, "Reflection of Thermal Cs Atoms Grazing a Polished Glass Surface," Phys. Rev. A: At., Mol., Opt. Phys. **34**, 3513 (1986).

27. O. Stern, "Beugung von Molekularstrahlen an Gitter einer Krystallspaltf," Naturwiss. **17**, 391 (1929).

28. O. R. Frish and O. Stern, "Anomalien bei der spiegelnden Reflektion und Beugung yon Molekularstrahlen an Kristallspaltfllichen: I," Z. Phys. **84**, 430 (1933).

29. D. W. Keith, M. L. Schattenburg, H. I. Smith, and D. E. Pritchard, "Diffraction of Atoms by a Transmission Grating," Phys. Rev. Lett. **61**, 1580 (1988).

30. J. J. Berkhout, O. J. Luiten, I. D. Setija, T. W. Hijmans, T. Mizusaki, and J. T. M. Walraven, "Quantum Reflection: Focusing of Hydrogen Atoms with a Concave Mirror," Phys. Rev. Lett. **63**, 1689 (1989).

31. O. Carnal, A. Faulstich, and J. Mlynek, "Diffraction of Metastable Helium Atoms by a Transmission Grating," Appl. Phys. B: Photophys. Laser Chem. **53**, 88 (1991).

32. M. Koch, S. Rehbein, S. Schmahl, T. Reisinger, G. Bracco, W. E. Ernst, and B. Holst, "Imaging with Neutral Atoms—A New Matter—Wave Microscope," J. Microsc. (Oxford) **229**, 1 (2008).

33. F. Shimizu, "Specular Reflection of Very Slow Metastable Neon Atoms from a Solid Surface," Phys. Rev. Lett. **86**, 987 (2001).

34. O. Carnal and J. Mlynek, "Young's Double-Slit Experiment with Atoms: A Simple Atom Interferometer," Phys. Rev. Lett. **66**, 2689 (1991).

35. D. W. Keith, C. R. Ekstrom, Q. A. Turchette, and D. E. Pritchard, "An Interferometer for Atoms," Phys. Rev. Lett. **66**, 2693 (1991).

36. H. Friedburg and W. Paul, "Reflexion eines Atomstrahles am Rande eines Magnetfeldes," Naturwiss. **37**, 20 (1950).

37. H. Friedburg and W. Paul, "Optische Abbildung mit neutralen Atomen," Naturwiss. **38**, 159 (1951).

38. M. I. Korsunskii and Ya. M. Fogel, "Focusing of a Molecular Beam by a Nonhomogeneous Magnetic Field," Zh. Eksp. Teor. Fiz. **21**, 25 (1951); Zh. Eksp. Teor. Fiz. **21**, 38 (1951).

39. R. Vanthier, C. R. Hebd. Seances Acad. Sci. **228**, 1113 (1949).

40. H. M. Goldenberg, D. Kleppner, and N. F. Ramsey, "Atomic Hydrogen Maser," Phys. Rev. Lett. **5**, 361 (1960).

41. W. Kaenders, F. Lison, A. Richter, R. Wynands, and D. Meschede, "Imaging with an Atomic Beam," Nature (London) **375**, 214 (1995).

42. M. Mützel, M. Müller, D. Haubrich, U. Rasbach, and D. Meschede, "The Atom Pencil: Serial Writing in the Sub-Micrometer Domain," Appl. Phys. B: Lasers Opt. **80**, 941 (2005).

43. G. Benewitz, W. Paul, and C. Schlier, "Fokussierung polarer Moleküle," Z. Phys. **141**, 6 (1995).

44. J. P. Gordon, H. J. Zeiger, and C. Townes, "The Maser—A New Type of Microwave Amplifier, Frequency Standard, and Spectrometer," Phys. Rev. **99**, 1264 (1955).

45. N. G. Basov and A. M. Prokhorov, "On Possible Methods of Producing Active Molecules for a Molecular Generator," Zh. Eksp. Teor. Fiz. **28**, 249 (1955) [Sov. Phys. JETP **1**, 184 (1955)].

46. M. Morinaga, "Focusing Ground State Atoms with an Electrostatic Field," Appl. Phys. B: Lasers Opt. **79**, 679 (2004).

47. J. G. Kalnins, J. M. Amini, and H. Gould, "Focusing a Fountain of Neutral Atoms with an Electrostatic Lens Triplet," Phys. Rev. A: At., Mol., Opt. Phys. **72**, 043 406 (2005).

48. A. Faulstich, A. Schnetz, M. Siegel, T. Sleator, O. Carnal, V. Balykin, H. Takuma, and J. Mlynek, "Imaging and Focusing of an Atomic-Beam with a Large Period Standing Light-Wave," Europhys. Lett. **17**, 393 (1992).

49. P. N. Melent'ev, P. A. Borisov, S. N. Rudnev, A. E. Afanas'ev, and V. I. Balykin, "Focusing of an Atomic Beam by a Two-Dimensional Magneto-Optical Trap," Pis'ma Zh. Eksp. Teor. Fiz. **83** (1), 16 (2006) [JETP Lett. **83** (1), 14 (2006)].

50. F. Lison, P. Schuh, D. Haubrich, and D. Meschede, "High-Brilliance Zeeman-Slowed Cesium Atomic Beam," Phys. Rev. A: At., Mol., Opt. Phys. **61**, 013 405 (1999).

51. C. Salomon, J. Dalibard, A. Aspect, H. Metcalf, and C. Tannoudji, "Channeling Atoms in a Laser Standing Wave," Phys. Rev. Lett. **59**, 1659 (1987).

52. V. I. Balykin, V. S. Letokhov, Yu. B. Ovchinnikov, A. I. Sidorov, and S. V. Shul'ga, "Channeling of Atoms in a Standing Spherical Light Wave," Opt. Lett. **13**, 958 (1988).
53. S. Chu, L. Hollberg, J. E. Bjorkholm, A. Cable, and A. Ashkin, "Three-Dimensional Viscous Confinement and Cooling of Atoms by Resonance Radiation Pressure," Phys. Rev. Lett. **55**, 48 (1985).
54. D. R. Meacher, "Optical Lattices—Crystalline Structures Bound by Light," Contemp. Phys. **39**, 329–350 (1998).
55. J. E. Bjorkholm, R. E. Freeman, A. A. Ashkin, and D. B. Pearson, "Observation of Focusing of Neutral Atoms by the Dipole Forces of Resonance-Radiation Pressure," Phys. Rev. Lett. **41**, 1361 (1978).
56. A. Ashkin and J. M. Dziedzic, "Optical Trapping and Manipulation of Viruses and Bacteria," Science (Washington) **235**, 1517 (1987).
57. M. Prentiss, G. Timp, N. Bigelow, R. E. Behringer, and J. E. Cunningham, "Using Light as a Stencil," Appl. Phys. Lett. **60** 1027 (1992); G. Timp, R. E. Behringer, D. M. Tennant, J. E. Cunningham, M. Prentiss, and K. K. Berggren, "Using Light as a Lens for Submicron, Neutral-Atom Lithography," Phys. Rev. Lett. **69**, 1636 (1992).
58. M. Mützel, D. Haubrich, and D. Meschede, "Nanoscale Focusing of Atoms with a Pulsed Standing Wave," Appl. Phys. B: Lasers Opt. **70** 689 (2000); M. Mützel, U. Rasbach, D. Meschede, C. Burstedde, J. Braun, A. Kunoth, K. Peithmann, and K. Buse, "Atomic Nanofabrication with Complex Light Fields," Appl. Phys. B: Lasers Opt. **77**, 1–9 (2003).
59. J. J. McClelland, R. E. Scholten, E. C. Palm, and R. J. Celotta, "Laser-Focused Atomic Deposition," Science (Washington) **262**, 877 (1993).
60. C. C. Bradley, W. R. Anderson, J. J. McClelland, and R. J. Celotta, "Nanofabrication via Atom Optics," Appl. Surf. **141**, 210–218 (1999).
61. J. J. McClelland and M. Prentiss, in *Nanotechnology*, Ed. by G. Timp (American Institute of Physics, Melville, NY, United States, 1999), Chapter 10.
62. M. K. Oberthaler and T. Pfau, "One-, Two-, and Three-Dimensional Nanostructures with Atom Lithography," J. Phys.: Condens. Matter **15**, R233 (2003).
63. D. Meschede and H. Metcalf, "Atomic Nanofabrication: Atomic Deposition and Lithography by Laser and Magnetic Forces," J. Phys. D: Appl. Phys. **36**, R17–R38 (2003).
64. J. J. McClelland, S. B. Hill, M. Pichler, and R. J. Celotta, "Nanotechnology with Atom Optics," Sci. Technol. Adv. Mater. **5**, 575 (2004).
65. V. I. Balykin, V. S. Letokhov, V. G. Minogin, Yu. V. Rozhdestvenskii, and A. I. Sidorov, "Collimation and Decollimation of Atomic Beams by Laser Radiation Pressure," Zh. Eksp. Teor. Fiz. **90** (3), 458 (1986) [Sov. Phys. JETP **63** (3), 508 (1986)].
66. J. Villain, A. Pimpinelli, L. Tang, and D. Wolf, "Terrace Sizes in Molecular Beam Epitaxy," J. Phys. I **2**, 2107–2121 (1992).
67. A. Pimpinelli, J. Villain, and D. E. Wolf, "Fractal Terraces in Molecular Beam Epitaxy Growth," J. Phys. I **3**, 447–457 (1993).
68. E. Te Sligte, K. M. R. van der Stam, B. Smeets, P. van der Straten, R. E. Scholten, H. C. W. Beijerinck, and K. A. H. van Leeuwen, "Barrier-Limited Surface Diffusion in Atom Lithography," J. Appl. Phys. **95** (4), 1749–1755 (2004).
69. A. Pimpinelli, J. Villain, and D. E. Wolf, "Fractal Terraces in MBE Growth," J. Phys. I **3**, 447–457 (1993).
70. E. Jurdik, Th. Rasing, H. van Kempen, C. C. Bradley, and J. J. McClelland, "Surface Growth in Laser-Focused Atomic Deposition," Phys. Rev. B: Condens. Matter **60**, 1543 (1999).
71. R. Gupta, J. J. McClelland, Z. J. Jabbour, and R. J. Celotta, "Nanofabrication of a Two-Dimensional Array Using Laser-Focused Atomic Deposition," Appl. Phys. Lett. **67** 1378 (1995); R. Gupta, J. J. McClelland, P. Marte, and R. J. Celotta, "Raman-Induced Avoided Crossings in Adiabatic Optical Potentials: Observation of $\lambda/8$ Spatial Frequency in the Distribution of Atoms," Phys. Rev. Lett. **76**, 4689 (1996).
72. K. K. Berggren, A. Bard, J. L. Wilbur, J. D. Gillaspy, A. G. Helg, J. J. McClelland, S. L. Rolston, M. Prentiss, and G. M. Whitesides, "Microlithography by Using Neutral Metastable Atoms and Self-Assembled Monolayers," Science (Washington) **269**, 1255 (1995).
73. S. J. Rehse, A. D. Glueck, S. A. Lee, A. B. Goulakov, C. S. Menoni, D. C. Ralph, K. S. Johnson, and M. Prentiss, "Nanolithography with Metastable Neon Atoms: Enhanced Rate of Contamination Resist Formation for Nanostructure Fabrication," Appl. Phys. Lett. **71**, 1427 (1997).
74. S. J. Rehse, A. D. Glueck, S. A. Lee, A. B. Goulakov, C. S. Menoni, D. C. Ralph, K. S. Johnson, and M. Prentiss, "Nanostructure Fabrication in Silicon Using Cesium to Pattern a Self-Assembled Monolayer," Appl. Phys. Lett. **71**, 1427 (1997).
75. R. E. Behringer, V. Natarajan, and G. Timp, "Optimal Profile for a Gaussian Standing-Wave Atom-Optical Lens," Opt. Lett. **22**, 114–116 (1997).
76. U. Drodofsky, J. Stuhler, Th. Schulze, M. Drewsen, B. Brezger, T. Pfau, and J. Mlynek, "Hexagonal Nanostructures Generated by Light Masks for Neutral Atoms," Appl. Phys. B: Lasers Opt. **65**, 755 (1997).
77. E. Jurdik, G. Myzkiewicz, J. Hohfeld, A. Tsukamoto, A. J. Toonen, A. F. van Etteger, J. Gerritsen, J. Hermsen, S. Goldbach-Aschemann, W. L. Meerts, H. van Kempen, and Th. Rasing, "Quasiperiodic Structures via Atom-Optical Nanofabrication," Phys. Rev. B: Condens. Matter **69**, 201 102 (2004).
78. M. Mützel, U. Rasbach, D. Meschede, C. Burstedde, J. Braun, A. Kunoth, K. Peithmann, and K. Buse, "Atomic Nanofabrication with Complex Light Fields," Appl. Phys. B: Lasers Opt. **77**, 1–9 (2003).
79. Th. Schulze, T. Müther, D. Jürgens, B. Brezger, M. Oberchaler, T. Pfau, and J. Mlynek, "Structured Doping with Light Forces," Appl. Phys. Lett. **78**, 1781 (2001); Th. Schulze, B. Brezger, R. Mertens, M. Pivk, T. Pfau, and J. Mlynek, "Writing a Superlattice with

Light Forces" Appl. Phys. B: Lasers Opt. **70**, 671–674 (2000).

80. E. Te Sligte, B. Smeets, R. C. M. Bosch, K. M. R. van der Stam, L. P. Maguire, R. E. Scholten, H. C. W. Beijerinck, and K. A. H. Leeuwen, "Progress towards Atom Lithography on Iron," Microelectron. Eng. **67–68**, 664 (2003); E. Te Sligte, B. Smeets, R. van der Stam, R. W. Herfst, P. van der Straten, H. C. W. Beijerinck, and K. A. H. van Leeuwen, "Atom Lithography of Fe," Appl. Phys. Lett. **85**, 4493 (2004).
81. G. Myszkiewicz, J. Hohlfeld, A. J. Toonen, A. F. van Etteger, O. I. Shklyarevskii, W. L. Meerts, and Th. Rasing, "Laser Manipulation of Iron for Nanofabrication," Appl. Phys. Lett. **85**, 3842 (2004).
82. R. Ohmukai, S. Urabe, and M. Watanabe, "Atomic Nanofabrication Using an Ytterbium Atomic Beam," Sci. Technol. Adv. Mater. **5**, 585 (2004).
83. S. J. Rehse, R. W. McGowan, and S. A. Lee, "Optical Manipulation of Group III Atoms," Appl. Phys. B: Lasers Opt. **70**, 657–660 (2000).
84. H. A. Bethe, "Theory of Diffraction by Small Holes," Phys. Rev. **66**, 163 (1944).
85. J. Meixner and W. Andrejewski, "Strenge Theorie die Beugung elektromagnetischer Wellen an der vollkommen leitenden Kreisscheibe und an der kreisförmigen Öffnung im vollkommen leitenden ebenen Schirm," Ann. Phys. (Weinheim) **7**, 157–168 (1950).
86. Y. Nomura and S. Katsura, "Diffraction of Electromagnetic Waves by Circular Plates and Circular Holes," J. Phys. Soc. Jpn. **10**, 285 (1955).
87. Y. Levitan, "Study of Near-Zone Fields of a Small Aperture," J. Appl. Phys. **60**, 1577–1583 (1986); V. V. Klimov and V. S. Letokhov, "A Simple Theory of the Near-Field in Diffraction by a Round Aperture," Opt. Commun. **106**, 154 (1994).
88. V. Balykin, V. Klimov, and V. Letokhov, "Laser Near-Field Lens for Atoms," J. Phys II **4**, 1981 (1994).
89. V. I. Balykin, V. S. Letokhov, and V. V. Klimov, "Tight Focusing of an Atomic-Beam by the Near-Field of Diffracted Laser-Light," Pis'ma Zh. Eksp. Teor. Fiz. **59** (4), 219 (1994) [JETP Lett. **59** (4), 235 (1994)].
90. V. I. Balykin, V. V. Klimov, and V. S. Letokhov, "Atom Nano-Optics Based on Photon Dots and Photon Holes," Pis'ma Zh. Eksp. Teor. Fiz. **78** (1), 11 (2003) [JETP Lett. **78** (1), 8 (2003)].
91. V. I. Balykin, V. S. Letokhov, and V. V. Klimov, "Atom Nano-Optics," Opt. Photonics News **4**, 33 (2005).
92. V. I. Balykin, V. G. Minogin, and S. N. Rudnev, "Atomic Beam Focusing by a Near-Field Atomic Microlenses," Zh. Eksp. Teor. Fiz. **130** (5), 784 (2006) [JETP **103** (5), 679 (2006)].
93. V. I. Balykin, "Atom Waveguides," Adv. At., Mol., Opt. Phys. **41**, 181 (1999).
94. R. Lüthi, R. R. Schlitter, J. Bruger, P. Vettriger, M. E. Welland, and J. K. Gimzewski, "Parallel Nanodevice Fabrication Using a Combination of Shadow Mask and Scanning Probe Methods," Appl. Phys. Lett. **75**, 1314 (1999).
95. M. V. Subbotin, V. I. Balykin, D. V. Laryushin, and V. S. Letokhov, "Laser Controlled Atom Waveguide as a Source of Ultracold Atoms," Opt. Commun. **139**, 107 (1997).
96. V. I. Balykin, P. A. Borisov, V. S. Letokhov, P. N. Melentiev, S. N. Rudnev, A. P. Cherkun, A. P. Akimenko, P. Yu. Apel', and V. A. Skuratov, "Atom "Pinhole Camera" with Nanometer Resolution," Pis'ma Zh. Eksp. Teor. Fiz. **84** (8), 544 (2006) [JETP Lett. **84** (8), 466 (2006)].
97. H. Oberst, S. Kasashima, V. Balykin, and F. Shimisu, "Atomic-Matter-Wave Scanner," Phys. Rev. A: At., Mol., Opt. Phys. **68**, 013 606 (2003).
98. J. Arcamone, M. A. F. van den Boogaart, F. Serra-Graells, J. Fraxedas, J. Brugger, and F. Pérez-Murano, "Full-Wafer Fabrication by Nanostencil Lithography of Micro/Nanomechanical Mass Sensors Monolithically Integrated with CMOS," Nanotechnology **19**, 305 302 (2008).
99. Y. T. Li, J. Zhang, Z. M. Sheng, J. Zheng, Z. L. Chen, R. Kodama, T. Matsuoka, M. Tampo, K. A. Tanaka, T. Tsutsumi, and T. Yabuuchi, "High-Energy Electrons Produced in Subpicosecond Laser-Plasma Interactions from Subrelativistic Laser Intensities to Relativistic Intensities," Phys. Rev. E: Stat., Nonlinear, Soft Matter Phys. **69**, 036 405 (2004).
100. C. F. Meyer, in *The Diffraction of Light, X-Rays, and Material Particles*, Ed. by J. W. Edwards (University of Chicago, Chicago, IL, United States, 1934).
101. R. N. Melentiev, A. V. Zablozkiu, D. A. Larshin, A. S. Baturin, and V. I. Balykin "Nanolithography Based on an Atom Pinhole Camera," submitted to Nanotechnology (2009).
102. P. Yu. Apel, I. V. Blonskaya, S. N. Dmitriev, O. L. Orelovitch, A. Presz, and B. A. Sartowska, "Fabrication of Nanopores in Polymer Foils with Surfactant-Controlled Longitudinal Profiles," Nanotechnology **18**, 305 302 (2007).
103. J. Li, D. Stein, C. McMullan, D. Branton, M. J. Aziz, and J. A. Golovchenko, "Ion-Beam Sculpting at Nanometer Length Scales," Nature (London) **412**, 166 (2001).

SPELL OK